AEDC-TR-67-238

POSTFLIGHT (AS-202) APOLLO COMMAND MODULE AERODYNAMIC SIMULATION TESTS

B. J. Griffith and D. E. Boylan
ARO, Inc.

March 1968

VON KÁRMÁN GAS DYNAMICS FACILITY
ARNOLD ENGINEERING DEVELOPMENT CENTER
AIR FORCE SYSTEMS COMMAND
ARNOLD AIR FORCE STATION, TENNESSEE

NOTICES

When U. S. Government drawings specifications, or other data are used for any purpose other than a definitely related Government procurement operation, the Government thereby incurs no responsibility nor any obligation whatsoever, and the fact that the Government may have formulated, furnished, or in any way supplied the said drawings, specifications, or other data, is not to be regarded by implication or otherwise, or in any manner licensing the holder or any other person or corporation, or conveying any rights or permission to manufacture, use, or sell any patented invention that may in any way be related thereto.

Qualified users may obtain copies of this report from the Defense Documentation Center.

References to named commercial products in this report are not to be considered in any sense as an endorsement of the product by the United States Air Force or the Government.

POSTFLIGHT (AS-202) APOLLO COMMAND MODULE AERODYNAMIC SIMULATION TESTS

B. J. Griffith and D. E. Boylan
ARO, Inc.

AF – AEDC
Arnold AFS Tenn

FOREWORD

The research reported herein was done at the request of the Arnold Engineering Development Center (AEDC), Air Force Systems Command (AFSC), under System 920E in cooperation with the NASA Manned Spacecraft Center, Houston, Texas.

The results presented were obtained by ARO, Inc. (a subsidiary of Sverdrup & Parcel and Associates, Inc.), contract operator of Arnold Engineering Development Center (AEDC), AFSC, Arnold Air Force Station, Tennessee, under Contract AF 40(600)-1200. The tests were conducted from December 1966 through May 1967, under ARO Project No. VT0744, and the manuscript was submitted for publication on October 13, 1967.

The authors wish to acknowledge contributions to this research work by many of their colleagues at the von Kármán Gas Dynamics Facility (VKF), AEDC. Among the many who assisted in this work, L. K. Ward of the Supersonic Branch (VKF), R. H. Burt of the Hypersonic Branch (VKF), W. R. Lawrence of the Aerophysics Branch (VKF), and W. S. Norman of the Hypervelocity Branch (VKF), contributed materially in obtaining and analyzing the experimental results. The authors are also grateful to Bass Redd and Ralph Graham of the NASA Manned Space Center for providing helpful information and encouragement during the course of the research and to Jack D. Moote of North American Aviation for providing the pertinent details of Apollo Spacecraft 011.

This technical report has been reviewed and is approved.

Donald H. Meyer
Major, USAF
AF Representative, VKF
Directorate of Test

Leonard T. Glaser
Colonel, USAF
Director of Test

ABSTRACT

A comprehensive postflight wind tunnel investigation of the Apollo Command Module was conducted to resolve several anomalies between flight (AS-202) and preflight aerodynamic data. Attention was focused on (1) simulating the actual vehicle "as flown", (2) obtaining consistent pitch plane force measurements in the angle-of-attack range $150 \leq \alpha \leq 180$ deg, (3) the effect of Mach number over a range of 3 to 20, (4) the effect of Reynolds number, and (5) possible sting effects. Results indicated that prior failure to duplicate the asymmetrical wavy heat shield in preflight testing resulted in a significant error in trim angle-of-attack prediction. In addition, a strong viscous influence was found to extend down to an altitude of about 220,000 ft. Also, a Mach number influence to a value of about 14 was found which is substantially higher than previous blunt body investigations have indicated.

CONTENTS

APPENDIXES

I. ILLUSTRATIONS

Figure

NOMENCLATURE

(See Fig. 2 for Sign Convention)

a_2	Speed of sound downstream of a Rankine-Hugoniot normal shock
C_∞	Chapman-Rubesin viscosity coefficient ($\mu_W/\mu_\infty = C_\infty T_W/T_\infty$)
C_A	Axial-force coefficient
C_D	Drag-force coefficient
C_L	Lift-force coefficient
C_N	Normal-force coefficient
$C_{m_{cg}}$	Pitching-moment coefficient referenced to Apollo Mission AS-202 CM center of gravity (see Fig. 2)
$C_{m_{cg_1}}$	Pitching-moment coefficient referenced to $e/d = 0.035$ and $\bar{x}/d = 0.2688$
$C_{m_{HS}}$	Pitching moment referenced to $e/d = 0$ and $\bar{x}/d = 0$
CM	Command Module
d	Maximum diameter of CM
e	Center-of-gravity offset from CM centerline (see Fig. 2)

e/d	Ratio of offset to CM diameter
$K_{n2,d}$	Knudsen number based on conditions downstream of a normal shock and CM diameter
L/D	Lift-to-drag ratio
M_2	Mach number downstream of a normal shock
M_∞	Free-stream Mach number
p	Local surface pressure
p_o'	Impact pressure
p_o	Stagnation pressure
$Re_{\infty,d}$	Free-stream Reynolds number based on CM diameter
Re_{2d}	Reynolds number downstream of a normal shock based on CM diameter
Re_{wd}	Reynolds number based on local flow and temperature at model surface and CM diameter
SA	Surviving antenna
T_o	Stagnation temperature
T_w	Wall temperature
T_∞	Free-stream temperature
U_2	Velocity downstream of a normal shock
U_∞	Free-stream velocity
UH	Umbilical housing
$\bar{v}_{\infty_d}$	Viscous interaction parameter defined as $M_\infty\left(C_\infty/Re_{\infty_d}\right)^{1/2}$
X	Distance aft of heat shield
$\bar{x}$	Center-of-gravity location measured longitudinally from aft heat shield (see Fig. 2)
$\bar{x}/d$	Ratio of longitudinal center-of-gravity location to CM diameter
α	Angle of attack, body axis
α_E	Effective angle of attack = $\sqrt{(180 - \alpha)^2 + \beta^2}$
α_T	Trim angle of attack
β	Angle of side slip, body axis
γ	Ratio of specific heats

θ	Measured angle of model referenced to the (x, z) plane of Range G
θ_b	Local inclination angle of body
λ_2	Mean free path downstream of a normal shock
μ_∞	Free-stream viscosity
μ_2	Viscosity downstream of a normal shock
μ_w	Viscosity based on wall temperature
ρ_∞	Free-stream density
ρ_2	Density downstream of a normal shock
σ	Shock inclination angle
ψ	Measured angle of model referenced to (x, y) plane of Range G

SECTION I
INTRODUCTION

The motion of a spacecraft in flight is determined by the propulsive forces supplied, the force of gravity, the inertial characteristics of the spacecraft, and the aerodynamic forces. The wind tunnel is generally recognized as being almost indispensable in obtaining the aerodynamic information necessary to predict the motion of the spacecraft. However, the validity of wind tunnel data depends on the minimization of the possible sources of error and the simulation of the flow around the spacecraft in flight. The purpose of this report is to present a direct comparison between flight and wind tunnel data pertaining to the Apollo Command Module (CM) during the re-entry phase. Attention is focused on (1) simulating Apollo spacecraft 011 (AS-202) "as flown" in model construction, * (2) obtaining consistent pitch plane force measurements in the angle-of-attack range of interest, (3) defining the effect of Mach number on the resulting aerodynamics of the spacecraft, (4) defining the effect of Reynolds number, and (5) possible sting effects.

The aerodynamic model data reported herein were obtained in the 40-in. supersonic Tunnel A, the 50-in. hypersonic Tunnels B and C, the 100-in. hypersonic Tunnel F, the low-density hypersonic Tunnel L, and the hypervelocity Range G (Gas Dynamic Wind Tunnels, Supersonic A, Hypersonic B, C, F, L, and 1000-ft Hypervelocity Range G) of the von Kármán Gas Dynamics Facility (VKF), Arnold Engineering Development Center (AEDC). Other Apollo wind tunnel data utilized in this report were taken from Ref. 1. The Apollo flight test results were obtained from Ref. 2.

A previous investigation (Ref. 3) on the Gemini re-entry spacecraft indicated how useful a systematic and carefully analyzed wind tunnel program could be in the prediction of flight aerodynamics of re-entry spacecrafts. The strong viscous effects which could be expected to influence the aerodynamics of blunt bodies during the initial portion of re-entry were reported in Ref. 4.

---

*The simulated shape was that of the spacecraft 011 before re-entry; the shape changes attributable to heat shield ablation were not simulated.

SECTION II
FLIGHT TEST PROGRAM

Apollo mission AS-201 was flown on February 26, 1966, to demonstrate the structural integrity of the spacecraft (009) and to evaluate heat-shield performance during re-entry (see Ref. 5). The spacecraft was not fully instrumented for re-entry flight aerodynamic data. In addition, a failure in the reaction control system resulted in a positive rolling re-entry rather than the planned lifting re-entry. Therefore, no comparisons between flight AS-201 and wind tunnel data are made in this report.

Apollo mission AS-202 was flown on August 25, 1966, using Spacecraft 011. A photograph of Spacecraft 011 prior to flight AS-202 is shown in Fig. 1. A considerable amount of detailed aerodynamic re-entry data resulted from this flight (Ref. 2). Inertial-platform accelerations and attitude angles were used in conjunction with a best-estimated trajectory, obtained from the onboard guidance and navigation system and from radar data, to calculate flight aerodynamic angles and force-coefficient ratios. Atmospheric data were obtained in the re-entry area. These measurements allowed a quantitative analysis between flight and preflight wind tunnel data to be made.

The sign conventions used in this report along with the equations for the lift and drag coefficients are presented in Fig. 2a. Figure 2b gives pertinent full-scale dimensions of the CM (also see Ref. 2).

A summary of pertinent aerodynamic flight data (AS-202) at high Mach numbers and preflight wind tunnel data is given in the following table:

		Remarks
cg Location		
$\bar{x}/d$	0.2703	See Fig. 2a
z/d	0.0039	
e/d	0.0338	
L/D		
Preflight	0.320	
Flight	0.27 - 0.30	
α_t, deg		Average trim angle at hypersonic Mach numbers
Preflight	159	
Flight	162.5	
Impact Point Error	205 n.m. uprange	AS-202 was lifting re-entry

With one exception, comparison of preflight Apollo CM aerodynamic data and actual flight AS-202 data was good. The one anomaly which resulted was the decreased flight L/D ratio. Postflight determination of the CM center of gravity confirmed the accurate determination of its location. The decreased flight L/D could then be traced to the fact that the vehicle trimmed at an angle of attack about 3.5 deg more than preflight moment data indicated. The resulting error in L/D was one reason that a large uprange error in splashdown position occurred. Figures 3 and 4 show altitude and flight parameters versus time from liftoff for the reentry of mission AS-202.

SECTION III
WIND TUNNEL PROGRAM

3.1 BRIEF HISTORY OF AWTTP (1962-1966)

The earlier Apollo Wind-Tunnel Testing Program (AWTTP), conducted prior to the present investigation, was established as part of the design and development program initiated in support of the Apollo spacecraft program. The AWTTP was designed to obtain the necessary aerodynamic data for detailed flight planning, flight analyses, and abort trajectories to meet various mission requirements. The tests were conducted in 25 different tunnels having Mach number range capabilities from near 0 to Mach number 19. The program was the responsibility of North American Aviation as prime spacecraft contractor. Moseley and Martino (Ref. 6) have given an excellent comprehensive chronological summary of the wind tunnel test program. Moseley, Moore, and Hughes (Ref. 1) present stability characteristics of the Apollo CM. A detailed summary of these two reports is beyond the scope of the present report. Rather, attention is drawn only to the Apollo Command aerodynamics in the attitude of heat shield forward, i.e., the re-entry attitude.

The CM aerodynamics are important since the spacecraft is designed to employ a low L/D ratio for flight path control during re-entry into the earth's atmosphere. Since the CM will experience a wide variation of flow regimes from high altitude, high Mach number flight to low altitude, low Mach number flight, many different facilities were employed in an effort to provide the necessary flow regimes. Reference 6 includes a tabulation of the various wind tunnel facilities employed in the investigation of the Apollo CM aerodynamics. In addition, two free-flight wind tunnel tests (Refs. 7 and 8) for which the heat shield was maintained in a forward attitude have been reported in the open literature. Primary parameters studied in these investigations were influence of model configuration, Mach number, and Reynolds number. Various studies have

been devoted to the influence of sting mount and base pressure effects, heat shield geometry, and center-of-gravity location.

3.2 BRIEF ANALYSIS OF DATA TAKEN UNDER THE AWTTP

Static stability data were taken over a Mach number range of 0.20 to ~19. Tests were made using both the smooth CM and models with surface modifications. These modifications included antennas, umbilical fairing (including pad 5 fairing), vent protuberances, and window and tower-leg cavities. However, on flight AS-202, the 205 miles uprange landing was in some part attributable to the aerodynamic performance of the spacecraft. The flight L/D ratio was significantly less than predicted. The primary reasons have been determined to be: (1) The actual heat shield asymmetry and surface condition of spacecraft 011 were different from that used in the preflight wind tunnel program. All wind tunnel models tested during the AWTTP had smooth symmetrical heat shields; (2) The high Mach number data taken during the AWTTP were taken early in the program. Both the Cornell Aeronautical Laboratory (CAL) Mach 15.8 data and the AEDC-VKF Mach 18.7 data were taken in 1962 (see Ref. 1). The accuracy of these data was such that high Mach number effects could not clearly be defined.

3.3 POSTFLIGHT (AS-202) WIND TUNNEL PROGRAM

A comprehensive wind tunnel program was undertaken in order to obtain additional wind tunnel data on the CM. Only the CM in the reentry attitude was tested in order that a systematic and carefully analyzed wind tunnel program could be completed in a short period of time. The program was a correlated effort between NASA and AEDC. Attention was focused on (1) simulating the actual vehicle "as flown" in model construction, (2) obtaining consistent pitch plane force measurements in the angle-of-attack range $150 \leq \alpha \leq$ deg, (3) the effect of Mach number over a range of from 3 to 20, (4) the effect of Reynolds number, and (5) possible sting effects. Table I presents a brief description of the wind tunnel program and the AEDC-VKF test facilities utilized during the investigation. The first test was initiated in Tunnel L during the month of December 1966. The final test entry was in Tunnel A during the month of May 1967. A detailed listing of nominal test conditions is shown in Table II.

3.4 FLIGHT AS-202 WIND TUNNEL MODELS

A number of models were constructed for use in the correlation program. The models ranged from 0.60 in. in diameter (heat shield) to

8.01 in. in diameter. For the Tunnels A, B, C, and F tests, the actual vehicle (spacecraft 011) "as flown" was simulated in model construction.* Detail templates drawn to model scale were furnished to AEDC by the North American Aviation Company. These templates were computer fairings of actual vehicle measurements (spacecraft 011) after installation of the ablation material over the heat shield and afterbody. Pertinent details of the spacecraft ablation heat shield configuration are shown in Fig. 5. Added ablation material on the windward surfaces of the spacecraft produces an asymmetrical configuration. Ablation material over the pressure pads (supporting structure) makes the heat shield wavy. Figure 6 shows a photograph of the models. A view of the asymmetrical wavy heat shield model produced by the classical Toepler-Schlieren technique is compared with the symmetrical heat shield model in Fig. 7. To the authors' knowledge, no previous experimental investigation has been considered concerning the asymmetrical wavy heat shield shown in Fig. 7. Both smooth symmetrical and asymmetrical wavy models were studied in the present investigation to provide consistent comparative data.

Pertinent model and sting measurements are presented in Fig. 8. The asymmetrical configurations were constructed according to the templates to station X/d = 0.30 (see Fig. 8). Hence, the symmetrical and asymmetrical configurations are identical aft of this station. Figure 9 gives the details of the umbilical fairing and surviving antenna. The nonsurviving antenna was not included on any of the models. The first series of tests in Tunnel F was inadvertently run with the umbilical housing upside down (at ϕ = 286 deg). However, no difference between the data for varying positions of the fairing could be noted. The Tunnel F asymmetrical model included only the umbilical housing, and the Tunnel L and Range G models were constructed with symmetrical heat shields and no protuberances because of scale limitations.

3.5 TEST FACILITIES FOR CURRENT INVESTIGATION

The current investigation was conducted in Tunnels A, B, C, F, L, and Range G.

Tunnel A is a continuous, closed-circuit, variable density, supersonic wind tunnel with a Mach number range of 1.5 to 6. The tunnel operates at stagnation pressures between 1.5 to 200 psia and stagnation temperatures of 70 to 290°F.

---

*The simulated shape was that of spacecraft 011 before re-entry; the shape changes attributable to heat shield ablation were not simulated.

Tunnel B (a continuous closed-circuit wind tunnel) operates at a nominal Mach number of 6 or 8 at stagnation pressures from 20 to 280 or from 50 to 900 psia, respectively, at stagnation temperatures up to 890°F.

Tunnel C (similar to Tunnel B) operates at a nominal Mach number of 10 or 12 at stagnation pressures from 200 to 2000 or from 600 to 2400 psia, respectively, at stagnation temperatures up to 1440°F. The data presented in this report at Mach 12 represent the first test (except for calibration) with the Mach 12 nozzle.

Tunnel F is an arc-driven hotshot-type wind tunnel with a 100-in. test section. Nitrogen, initially confined in an arc chamber by a diaphragm located near the throat of an attached 8-deg conical nozzle, is heated and compressed by an electric arc discharge and expanded through the conical nozzle to the test section. A useful run time between 50 and 100 msec is attained.

Tunnel L is a low density, hypersonic, continuous flow, arc heated, ejector-pumped facility, normally using nitrogen or argon as the test gas. Nitrogen was used for all the tests reported herein. Contoured nozzles provide gradient free flow at nominal Mach numbers of 4, 9, and 10 at varying free-stream Reynolds numbers.

Range G is a 1000-ft-long, 10-ft-diam, variable density tube wholly contained within an underground tunnel. Launching capability ranges from in-gun weights of 498 gm at 12,000 ft/sec to 130 gm at 23,000 ft/sec. Instrumentation includes provisions for pressure and temperature measurements, 43 dual-axis shadowgraph stations, schlieren photography, microwave and R-F cavity measurements, radiometric and spectrographic measurements, and high speed photography.

3.6 PROCEDURE

The broad range of flight conditions during flight AS-202 demanded that several of the AEDC-VKF tunnels be utilized. In order to keep the experimental program to a minimum, the results of a completed test entry were analyzed before the next test was started. For example, tests in Tunnel L were started prior to the Tunnel F tests in order to determine the viscous influence at simulated altitudes up to 350,000 ft. These tests resulted in a more meaningful experimental program in Tunnel F. However, the AEDC-VKF postflight tests still required 515 hr of testing. Selected basic data from the present investigation are plotted in Appendix II and tabulated in Table III. A summary of the testing program is as follows:

1. Viscous Effects at High Simulated Altitudes

   Tests were conducted in Tunnel L at Mach numbers of 9.37 and 10.15. The free-stream Reynolds number (based on heat shield diameter) ranged between 234 and 1283 by varying test conditions and model size. These tests were conducted during the period of 5 December 1966 to 9 January 1967.

2. Viscous and Mach Number Effects at Simulated Altitudes of 220,000 to 280,000 ft, plus a Study of the Influence of the Ablator (Heat Shield Geometry)

   These tests were conducted during the period of 26 December 1966 to 24 January 1967 in Tunnel F. Data were obtained over a Mach number range of 14.6 to 20 at free-stream Reynolds numbers of 13,700 to 377,000.

3. Viscous and Mach Number Effects at Simulated Altitudes of 150,000 to 200,000 ft, plus a Study of the Influence of the Ablator (Heat Shield Geometry)

   The first tests were conducted at Mach 8 in Tunnel B over a Reynolds number range ($Re_{\infty, d}$) of 0.36×10^6 to 1.8×10^6 on 17 January 1967. The tests were conducted using a small amplitude (±3 deg), free-oscillation, cross-flexure pivot balance in order to better define the trim angle. The data indicated the need for force coefficients at similar conditions. Additional tests were conducted on 23 February 1967 with a six-component, force-type, strain-gage balance.

4. Additional Data in the High Mach Number, Low Reynolds Number Range

   Additional data were obtained in Tunnel F during the week of 15 February 1967 in order to better define the variation of the Apollo force and moment coefficients with Reynolds number.

5. Verification of the Apparent Mach Number Effect

   Tests were conducted in Tunnel A on 18 May 1967 at Mach 3, 4, and 6 and on 26 May 1967 in Tunnel C at Mach 12. These data were necessary in order to better define the effect of Mach number on the force and moment coefficients of the CM.

6. Sting Effects

   Concurrent with the tests on the sting mounted models, configurations with the symmetrical smooth heat shield were being launched in Range G in order to study any possible influence of the sting. Shots were made with models that had full cg offsets (same as spacecraft AS-202), half cg offsets, and

zero cg offsets. The shots were made as near as possible to the Tunnel B test conditions and were made from 25 January to 25 March 1967.

3.7 ACCURACY AND REPEATABILITY

The accuracy of the data is, of course, a function not only of the uncertainty of the direct measurements but also of the test section flow properties. Except for the Mach 6 data in Tunnel A, the wind tunnel test section static temperatures were kept above the theoretical liquefaction value in order to add validity to the calculated flow properties. Assessments of the estimated uncertainties in individual data points are as follows:

	C_A	C_D	C_N	C_m	α_T, deg
Tunnel A	±0.01	±0.01	±0.002	±0.0012	---
Tunnel B	±0.01	±0.01	±0.002	±0.0012	---
Tunnel C	±0.01	±0.01	±0.002	±0.0012	---
Tunnel F	±0.03	±0.04	±0.005	±0.0018	---
Tunnel L	±0.03	±0.03	±0.02	±0.0025	---
Range G	---	±0.02	---	---	±1.2

SECTION IV
WIND TUNNEL CORRELATION PARAMETER

The comparison of wind tunnel or range data with flight data requires the determination of a suitable correlation parameter. The need for a correlation parameter, of course, is attributable to the fact that flight conditions and model size can seldom be duplicated in the wind tunnel.

Viscous effects are sometimes scaled using free-stream Reynolds number as the scaling parameter, but it is well known that this is not always the best procedure. Higher altitude viscous interaction effects have been successfully accounted for using the parameter $\bar{v}_\infty$ (Ref. 9 and 10). Both an Re_∞ and $\bar{v}_\infty$ parameter appear to be applicable to either blunt or sharp slender bodies or for configurations for which viscous effects are of second-order importance. However, the flow field of interest about a very blunt body such as the Apollo CM is the flow which is separated from the free stream by the bow shock wave.

If the bow shock is strong everywhere ($M_\infty \sin \theta_b \gg 1$), the density ratio ϵ approaches the limit $(\gamma - 1)/(\gamma + 1)$, and the flow quantities

immediately behind the shock become dependent upon only ρ_∞, U_∞, and σ.* In addition, the local Mach number downstream of a normal shock M_2 is always a low subsonic value with only about a 2-percent variation between M_∞ = 10 and 25. The shock Reynolds number Re_{2d} may be expressed as

$$Re_{2d} = \rho_2 U_2 d/\mu_2$$

$$= (\rho_\infty U_\infty d)/\mu_2$$

where d is the characteristic length chosen as the diameter of the heat shield in the present case.

Very high altitude rarefaction effects can be shown to be inversely proportional to the shock Reynolds number by noting:

$$Kn_{2d} = \lambda_2/d = (\pi\gamma/2)^{1/2} \mu_2/\rho_2 a_2 d$$

which reduces to

$$Kn_{2d} = 1.483\, M_2/Re_{2d}$$

where γ = 1.4. For free-stream Mach numbers of practical interest ($10 \leq M_\infty \leq 25$), the local Knudsen number may be expressed as

$$Kn_{2d} \simeq 0.569/Re_{2d}$$

to an accuracy of about ±1 percent.

An improved parameter would be one which would account for wall temperature effects (Ref. 11) such as:

$$Re_{wd} = (Re_{2d})\, \mu_2/\mu_w$$

However, lack of accurate wind tunnel and flight wall temperature values and the fact that

$$(\mu_\infty/\mu_w)_{\text{wind tunnel}} \sim (\mu_\infty/\mu_w)_{\text{flight}}$$

in the present case suggests that Re_{2d} should be an adequate correlation parameter between flight and wind tunnel data as long as the free-stream Mach number is high. Flight values of Re_{2d} for mission AS-202 are shown in Fig. 10. The velocity profile from the flight data was used in conjunction with the 1962 standard atmosphere and the viscosity values of Ref. 12 and Ref. 13 for the calculation of Re_{2d}. Calculations based on flight values of free-stream pressure and temperature gave essentially the same results. For the flight data, real gas normal shock relationships from Lewis and Burgess (Ref. 13) were employed. VKF wind

*Neglects effects of shock and boundary layer merging at the higher simulated altitudes.

tunnel data reduction programs include calculation of shock Reynolds number. Nominal facility test conditions obtained during the present investigation are indicated in Fig. 10 and tabulated in Table II to illustrate the regions of flight simulation achieved. Figure 11 compares both the Mach number (M_∞) and Reynolds number variation (Re_{2d}) of mission AS-202 with the facility test conditions. Note that although a variation of nearly five orders of magnitude in Reynolds number is shown, actual Mach number and Reynolds number simulation are achieved only at M_∞ = 6 and 8. However, it will be shown that this lack of simulation, although undesirable, is not serious.

The basis of the correlation presented in this report is illustrated in Fig. 12. When the pitching-moment data from the present investigation at a given angle of attack are plotted versus Re_{2d}, a consistent trend at values of Re_{2d} above 10^4 does not exist. However, plotting the same data ($Re_{2d} > 10^4$) versus Mach number presents a consistent variation. The other aerodynamic data (C_N, C_A) on the Apollo CM exhibit similar trends. The wind tunnel data at values of $Re_{2d} < 200$ were at Mach numbers of 9.4 and 10.2 (see Fig. 11). However, the strong viscous effects in this regime should make variations in free-stream Mach number rather insignificant.

These observations indicate that Apollo flight AS-202 aerodynamic data should be correlated on the basis of Re_{2d} down to an altitude of 177,000 ft ($M_\infty > 14$) and on Mach number below this altitude ($Re_{2d} > 10^5$).

SECTION V
WIND TUNNEL DATA CORRELATION AND COMPARISONS

The AEDC-VKF data are correlated over a free-stream Reynolds number range of 234 to 1.9×10^6 based on heat shield diameter and a Mach number range of 2.98 to approximately 20. The resulting correlations are shown in Figs. 13 through 15. The data points presented represent fairings of the basic data.

Figure 13 shows the variation of the axial-force coefficient of the Apollo CM with Re_{2d} and Mach number. Note the significant increase in C_A at values of Re_{2d} below 1000 and the slight increase at the lower free-stream Mach numbers. The reference area of the symmetrical smooth heat shield is used in data reduction which, in part, accounts for the higher axial force of the asymmetrical wavy heat shield configuration. Model scale limitations did not permit the asymmetrical wavy heat shield to be studied at low values of Re_{2d}. Therefore, the aerodynamics of the

symmetrical and asymmetrical models are assumed to be identical below a Re_{2d} of 200 since viscous effects should dominate in this flow regime.

The normal-force coefficient (C_N) is presented in Fig. 14. Viscous effects are significant below a Re_{2d} value of about 7000, whereas variations of C_N attributable to Mach number are generally slight. The asymmetrical wavy heat shield causes a decrease in the normal force (C_N) only at angles of attack between 170 and 180 deg.

Significant variations in the pitching moment ($C_{m_{cg}}$) of the Apollo CM with Reynolds number, Mach number, and heat shield configuration are shown in Fig. 15. The effect of the asymmetrical wavy heat shield is greater at the high Mach number-high Reynolds number flight condition ($M_\infty \geq 14$ and $Re_{2d} \geq 5000$) which represents a major portion of Apollo flight AS-202. Additional data in this important test regime would have been helpful. The strong viscous effect on pitching moment can be observed in Fig. 16, where the reference point is the most forward point on the heat shield centerline.

The effect of the normal shock Reynolds number (Re_{2d}) on L/D ratio of the Apollo CM is shown in Fig. 17. At a given angle of attack, over a 40-percent decrease is noted in L/D between a simulated altitude of 130,000 and 350,000 ft. The figure illustrates the importance of viscous effects at high altitudes.

In order to determine if the wind tunnel data were free of significant sting effects, several models were launched in the 1000-ft Range G at AEDC-VKF. Figure 18 is a photographic history of a typical Range G shot. Figure 19a shows the variation of α and β as the model flies downrange, during shot 620. Figure 19b presents the same shot in terms of the measured range angles θ and ψ. A second-order computer fit of the data is shown to illustrate the typical data fit. A comparison of the free-flight Range G data with the wind tunnel data is shown in Fig. 20. Note the good agreement and thus apparent lack of sting effects. Also, Fig. 21 compares the low density free-flight data of Horstmann and Kussoy (Ref. 7) from the Ames 1-ft shock tunnel with the present sting mount data from AEDC-VKF Tunnel L. Again, no apparent effect of the sting is noted.

Comparisons of the present symmetrical heat shield data with the previous data of Moseley, Moore, and Hughes (Ref. 1) are given in Fig. 22. Generally, good agreement is noted.

Balance cavity pressures were measured during the Tunnel A, B, C, and F test entries in order to monitor the flow in the base region of the model. In addition, a windward and leeward pressure on the afterbody were measured during the Tunnel F test entry. Figure 23 presents selected data from these measurements. No trend with Reynolds number or Mach number on the leeward or windward surface is noted, possibly indicating that the flow remained separated over the aft portion of the re-entry module.

SECTION VI
APOLLO FLIGHT-WIND TUNNEL DATA COMPARISONS

A comparison between the Apollo AS-202 flight trim angle of attack and wind tunnel data is presented in Fig. 24a. Note the good agreement of the asymmetrical wavy model wind tunnel data with the flight test data over the regime of trimmed flight. The correlation was made by using Re_{2d} as the correlation parameter from re-entry to an altitude (177,000 ft) at which $M_\infty = 14$ was reached and a Mach number correlation below this altitude. The correlation curves were obtained by cross plots of Fig. 15. The flight test data were obtained from the paper by Hillje (Ref. 2). The postflight symmetrical model correlation along with the preflight estimate (Ref. 2) are given for completeness. The preflight estimate was based on previous symmetrical model data. A summary of C_N/C_A and the L/D ratios for Flight AS-202 is shown in Figs. 24b and c. Again, good agreement is noted between the flight and asymmetrical wavy model wind tunnel data. The offset cg of spacecraft 011 changes during the final re-entry phase attributable, in part, to fuel usage. The effect of this variation on the correlated wind tunnel data is also shown in Figs. 24 and 25.

Figure 25 compares the present trim angle of attack and corresponding L/D to Apollo Mission AS-202 flight data. However, the comparison is shown in terms of Re_{2d} and M_∞ rather than flight time, as shown in Fig. 24, to illustrate the strong viscous influences found in the present study. Typical flight data from Mission AS-202 are tabulated in Table IV.

In order to demonstrate the extreme sensitivity of the aerodynamic characteristics of the Apollo CM to variations in flow regimes and cg location, Fig. 26 was constructed from the present data. Three flow conditions were selected to represent the range encountered as the CM reenters the earth's atmosphere. The data were then referenced to various

e/d and $\bar{x}$/d locations with the resulting curves shown in Fig. 26. Included are the experimentally determined L/D ratios as a function of angle of attack at the three flow conditions selected. For a center-of-gravity location corresponding to the AS-202 flight, an L/D variation from 0.320 to 0.225 (30 percent) could be expected over the flow regime selected. Newtonian calculations would give a 10-percent increase in L/D attributable to the trim angle change from 159.4 to 157.4. Hence viscous effects cause a 40-percent decrease in L/D over the selected regime. Figure 17 clearly illustrates the strong viscous influence on L/D.

SECTION VII
CONCLUDING REMARKS

A post-flight investigation was undertaken in order to obtain static stability characteristics of the Apollo CM "as flown" during flight AS-202. The principal conclusions of the investigation can be summarized as follows:

1. The influence of the ablator (heat shield) geometry causes a significant change in trim angle of attack and thus a decrease in available L/D ratio.
2. Wind tunnel data indicate that a very strong viscous influence exists on the Apollo CM in the initial portion of re-entry extending down to a simulated altitude of about 220,000 ft.
3. The Mach number influence extends to a value of about 14, which is substantially higher than previous blunt body investigations have indicated.
4. Based on the agreement between wind tunnel data, where real gas effects were not simulated, and full-scale flight data, where real gas effects were present, it may be concluded that real gas effects are not significant on the static stability of the Apollo CM at velocities up to 27,000 ft/sec.

REFERENCES

1. Moseley, William C., Jr., Moore, Robert H., Jr., and Hughes, Jack E. "Stability Characteristics of the Apollo Command Module." NASA TN D-3890, March 1967.
2. Hillje, Ernest R. "Entry Flight Aerodynamics from Apollo Mission AS-202." NASA TN D-4185, October 1967.

3. Griffith, B. J. "Comparison of Aerodynamic Data from the Gemini Flights and AEDC-VKF Wind Tunnels." AIAA Journal of Spacecraft, Vol. 4, No. 7, pp. 919-924, July 1967.

4. Boylan, David E. and Potter, J. Leith. "Aerodynamics of Typical Lifting Bodies under Conditions Simulating Very High Altitudes." AIAA Journal, Vol. 5 , No. 2, pp. 226-232, February 1967.

5. Postlaunch Report for Mission AS-201, MSC-A-R-66-4, May 6, 1966.

6. Moseley, William C., Jr., and Martino, Joseph C. "Apollo Wind Tunnel Testing Program-Historical Development of General Configurations." NASA TN D-3748, December 1966.

7. Horstmann, C. C. and Kussoy, M. I. "Free-Flight Measurements of Aerodynamic Viscous Effects on Lifting Re-Entry Bodies." AIAA Paper No. 67-165, Presented at the 5th Aerospace Sciences Meeting, January 23, 1967.

8. Seiff, Alvin. "Current and Future Problems in Earth and Planetary Atmosphere Entry." AIAA Paper No. 67-803, October 1967.

9. Whitfield, J. D. and Griffith, B. J. "Viscous Drag Effects on Slender Cones in Low-Density Hypersonic Flow." AIAA Journal, Vol. 2, No. 6, June 1965, pp. 1165-1166.

10. Whitfield, Jack D. and Griffith, B. J. "Hypersonic Viscous Drag Effects on Blunt Slender Cones." AIAA Journal, Vol. 2, No. 10, October 1964, pp. 1714-1722.

11. Potter, J. Leith. "The Transitional Rarefied-Flow Regime." Rarefied Gas Dynamics (C. L. Brundin, ed.), Vol. 2, pp. 881-937, Academic Press, New York, 1967.

12. Yos, Jerrold M. "Transport Properties of Nitrogen, Hydrogen, Oxygen, and Air to 30,000°K." AVCO Report RAD-TM-63-7, March 1963.

13. Lewis, Clark H. and Burgess, E. G., III. "Altitude Velocity Table and Charts for Imperfect Air." AEDC-TDR-64-214 (AD454078), January 1965.

APPENDIXES

I. ILLUSTRATIONS
II. BASIC DATA PLOTS
III. TABLES

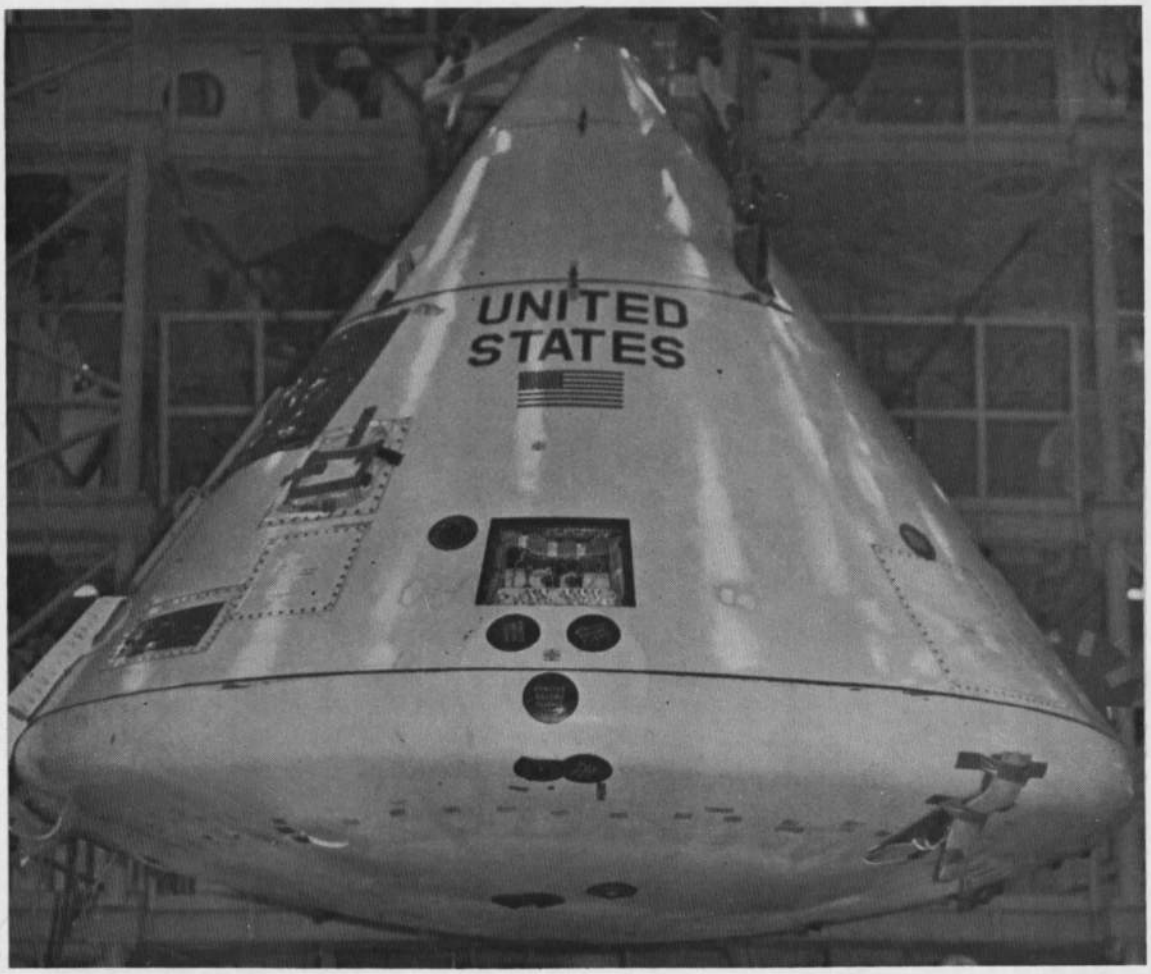

Fig. 1 Photograph of Spacecraft 011 Prior to Mission AS-202

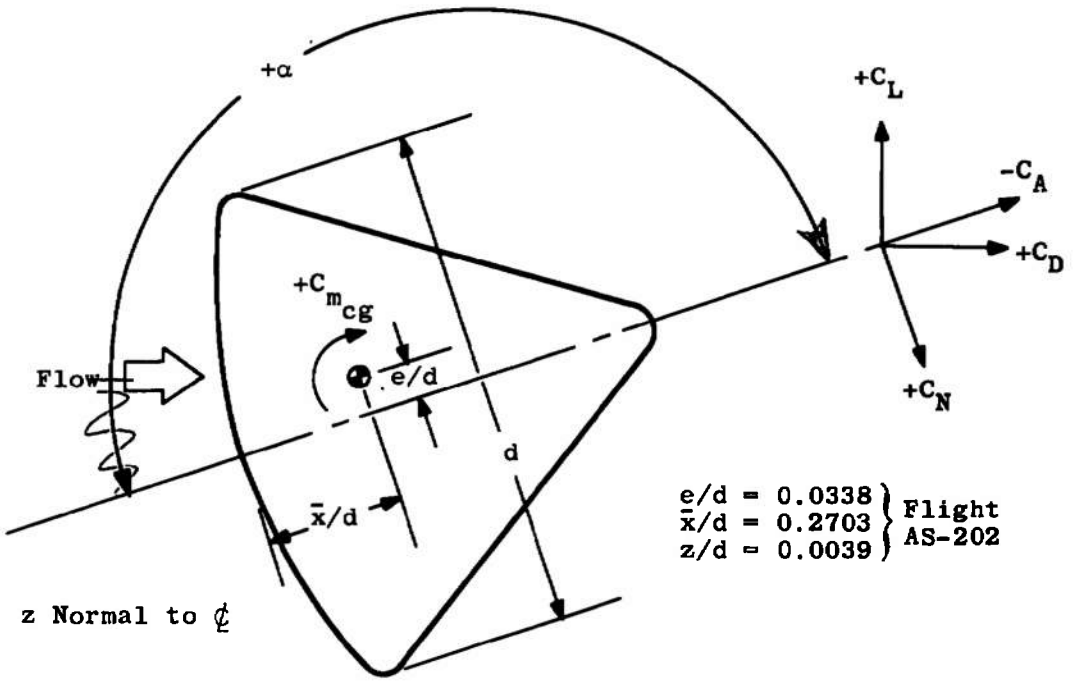

$C_D = C_N \sin (180 - \alpha) - C_A \cos (180 - \alpha)$

$C_L = - C_N \cos (180 - \alpha) - C_A \sin (180 - \alpha)$

a. Orientation of Forces and Moments

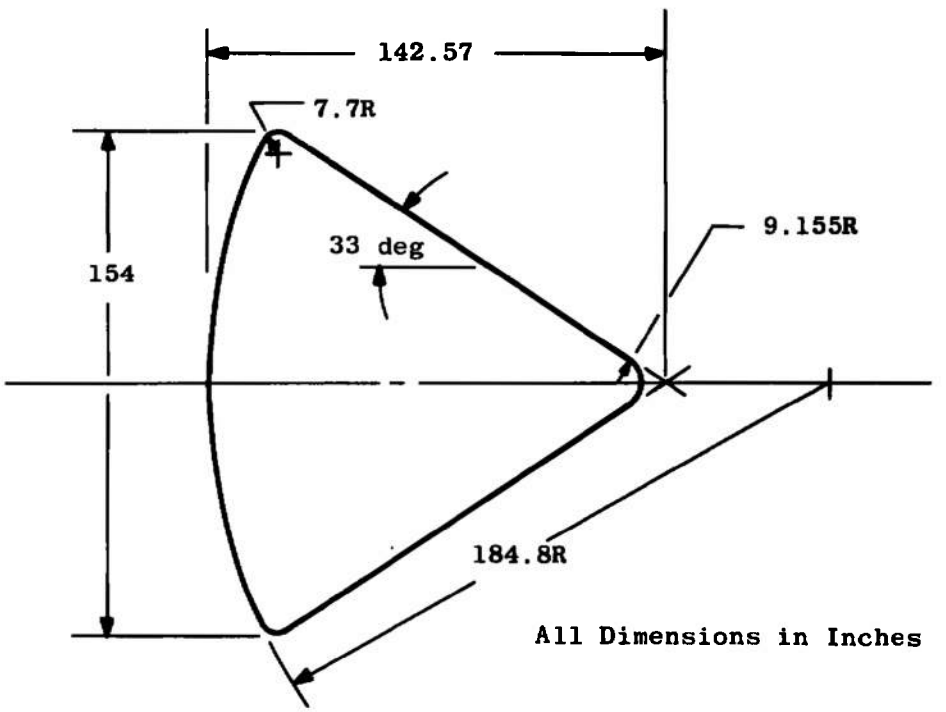

b. Apollo Spacecraft (Symmetrical Smooth Heat Shield Dimensions)

Fig. 2 Apollo CM Forces and Dimensions

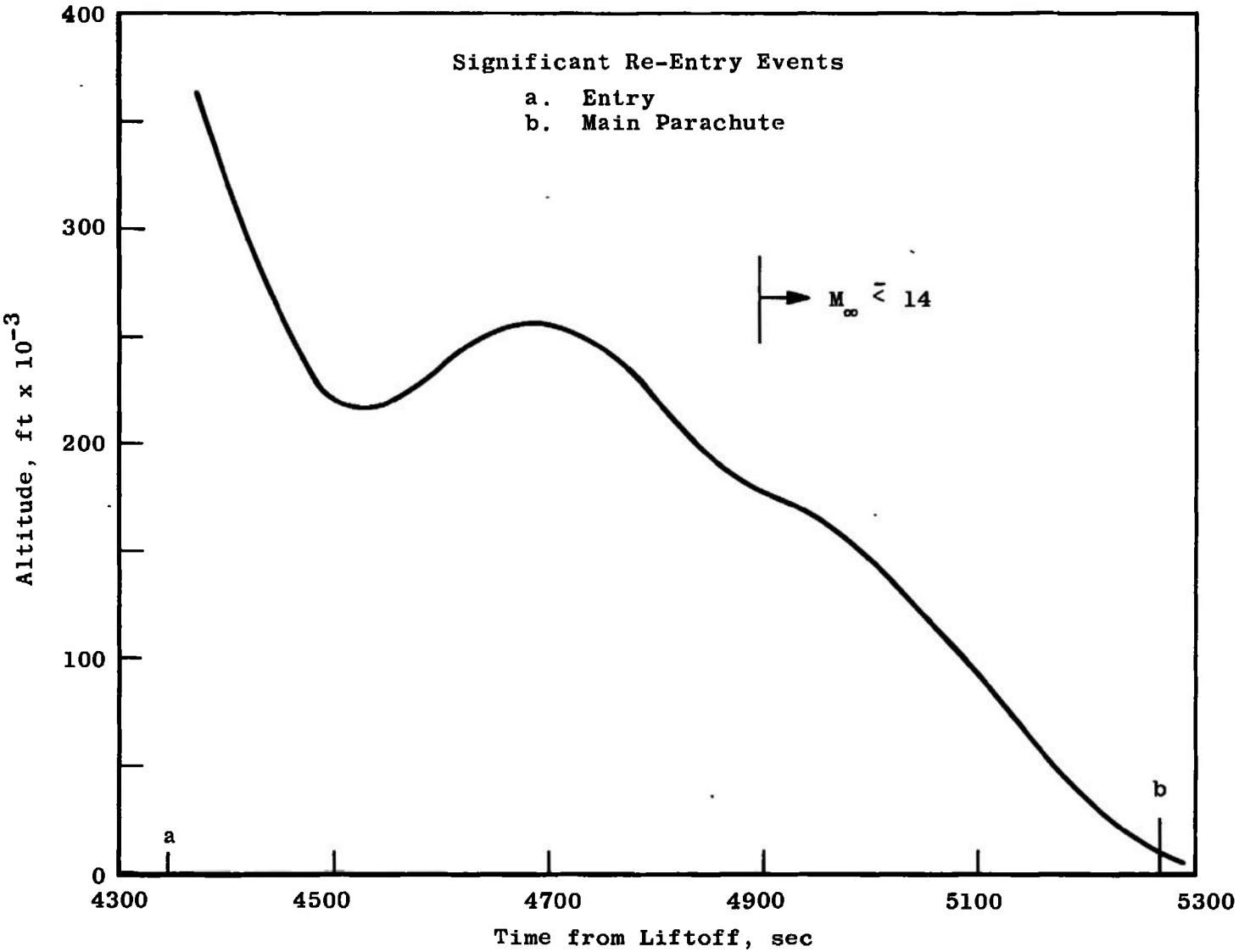

Fig. 3 Time History of Apollo Mission AS-202

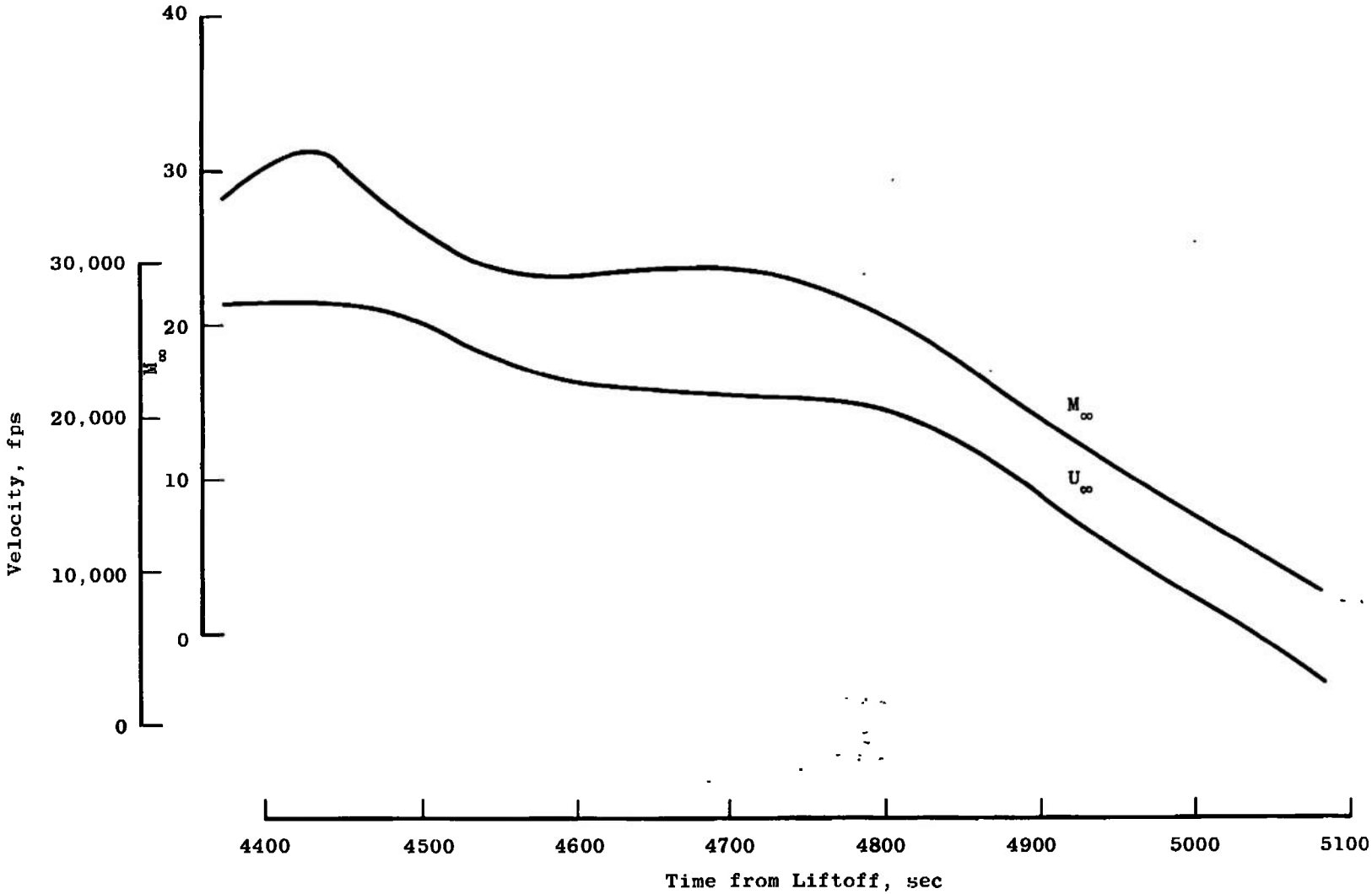

Fig. 4 Re-Entry Flight Parameters for Apollo Mission AS-202

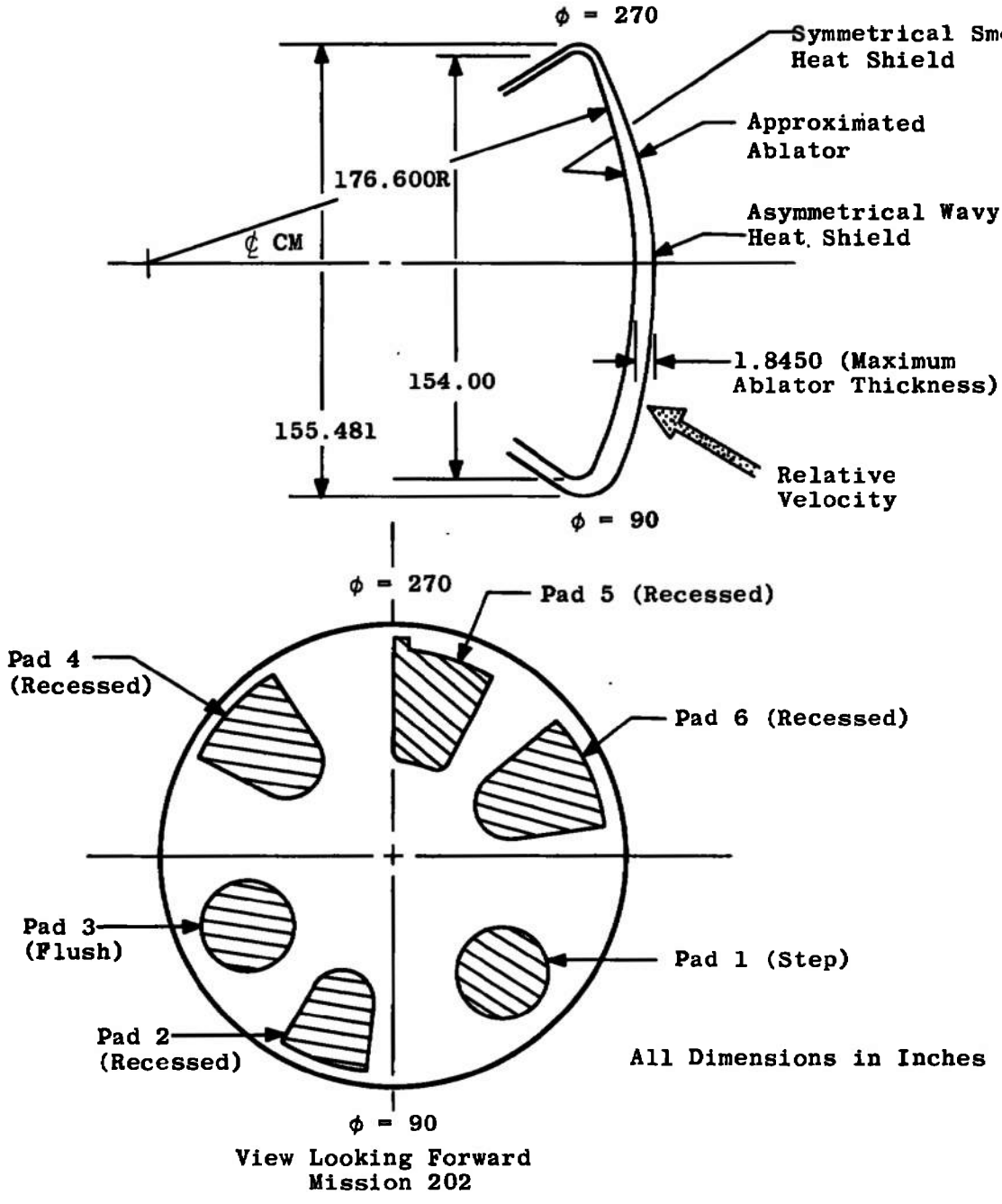

Fig. 5 Apollo Heat Shield Asymmetry

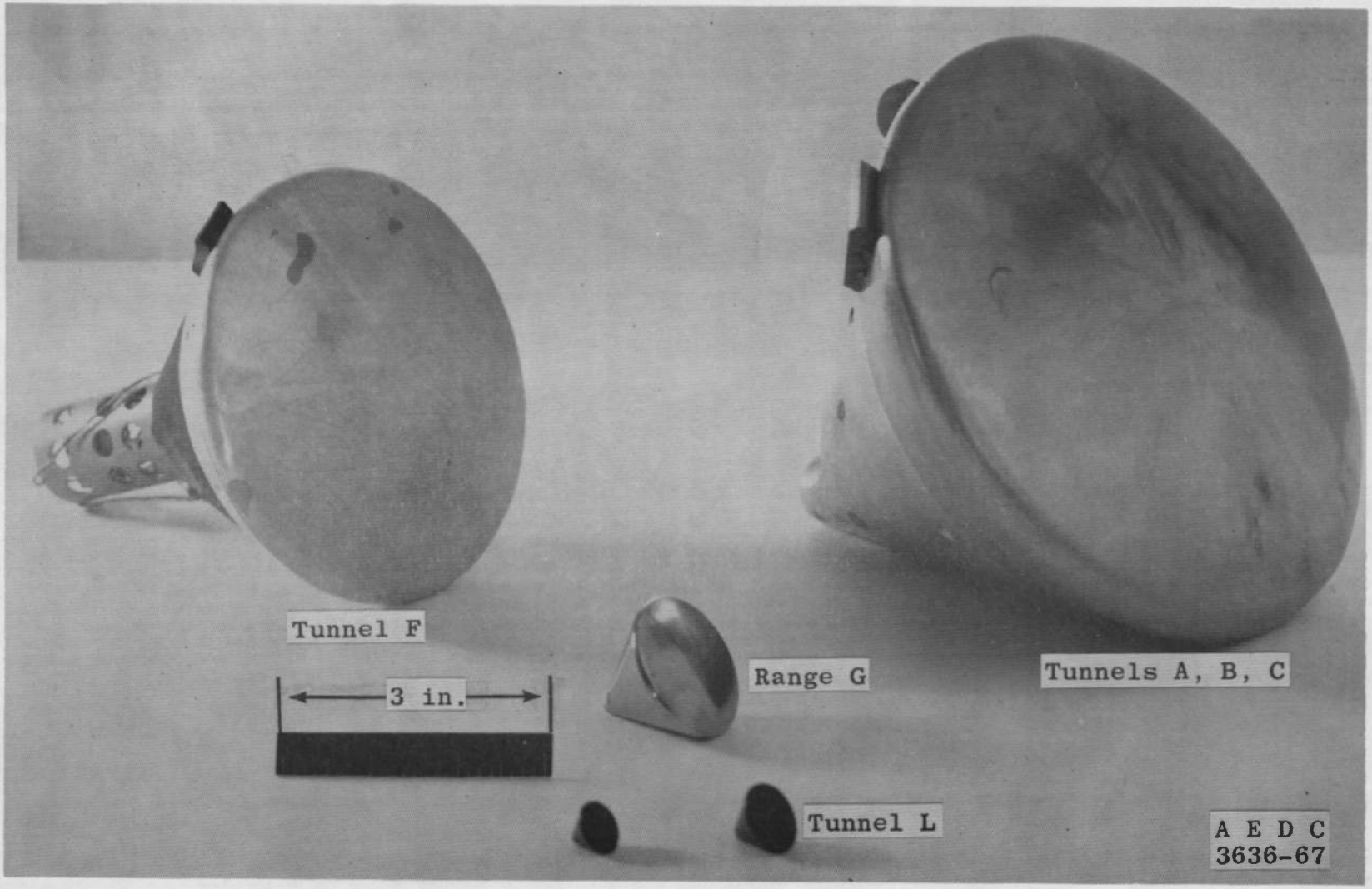

Fig. 6 Apollo Models

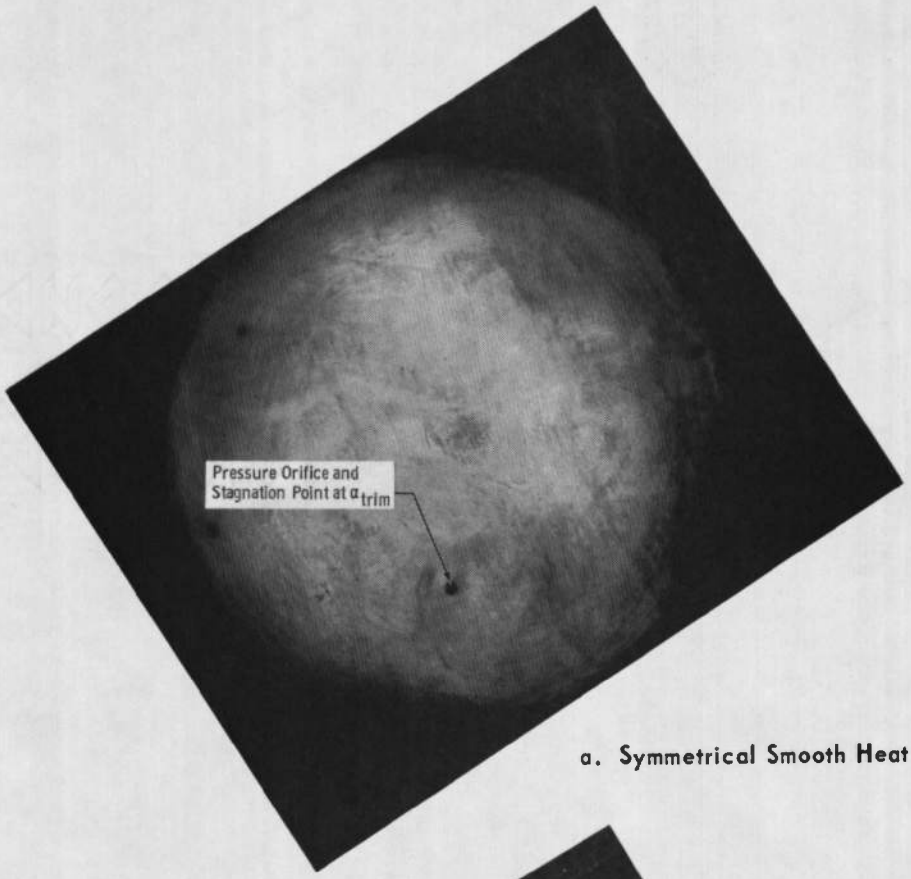

a. Symmetrical Smooth Heat Shield

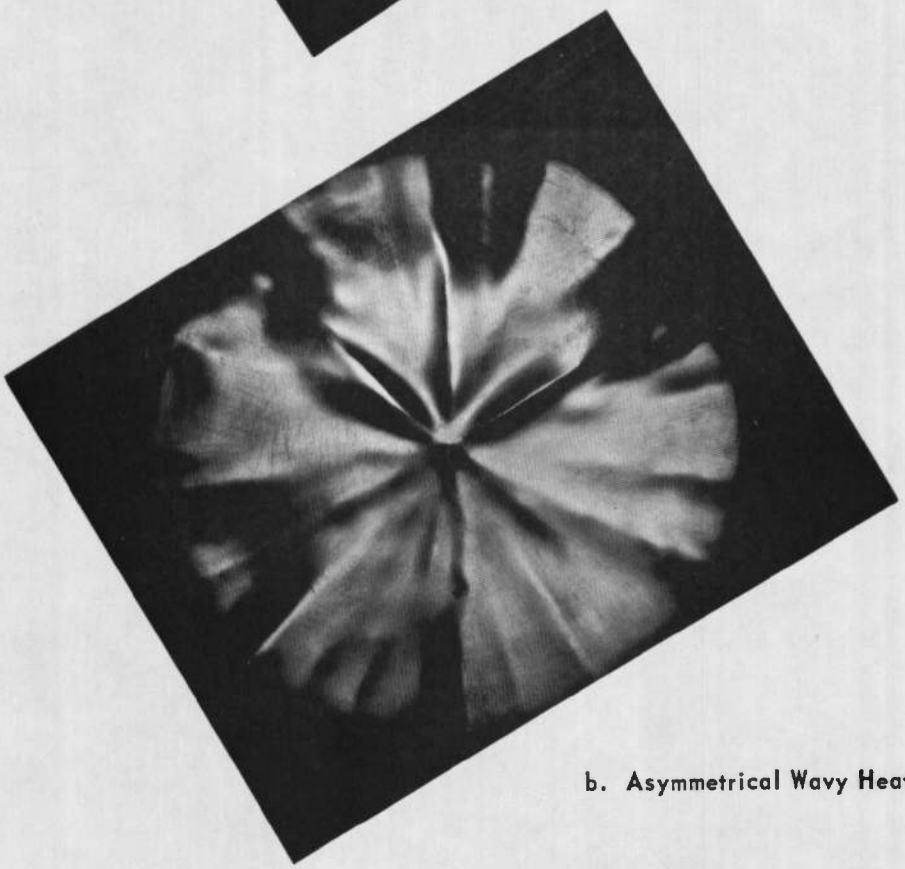

b. Asymmetrical Wavy Heat Shield

Fig. 7 Toepler-Schlieren Photograph of Face of Tunnel F Models

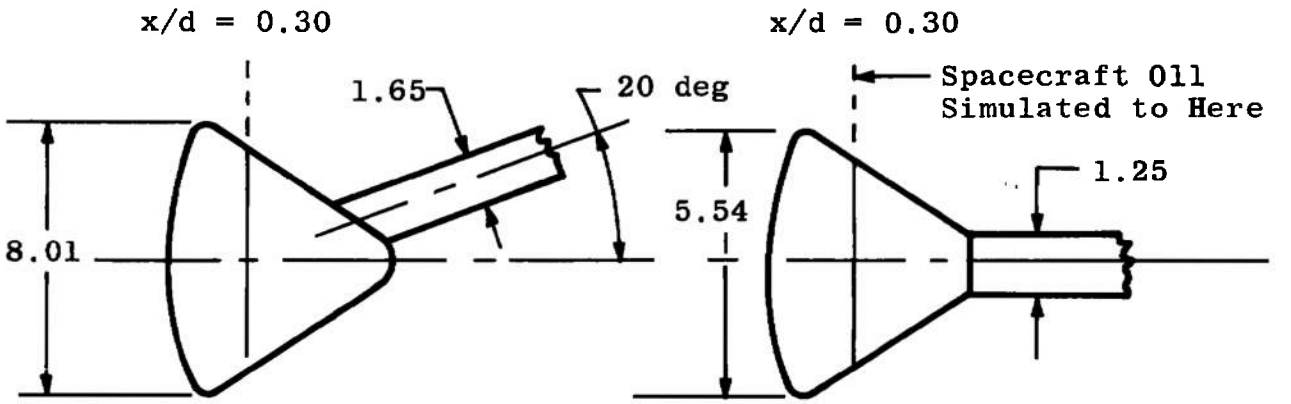

Tunnels A, B, and C

Smooth Heat Shield and Asymmetrical Wavy Heat Shield

Tunnel F

Smooth Heat Shield and Asymmetrical Wavy Heat Shield

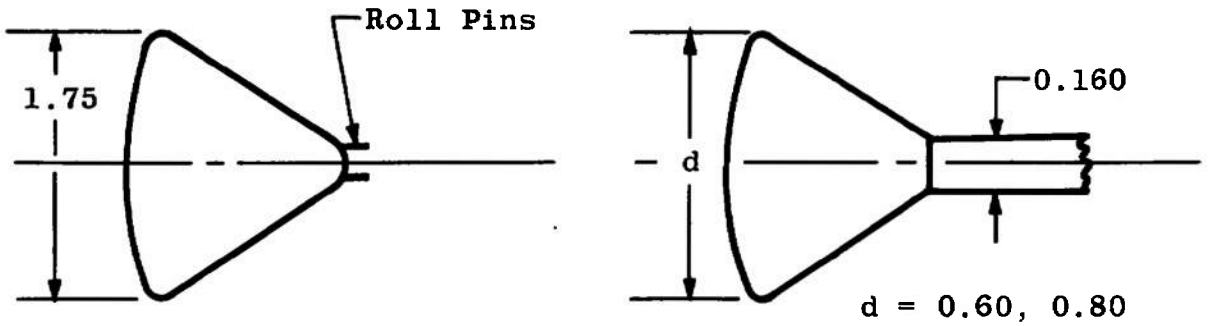

Range G

Smooth Heat Shield

Tunnel L

Smooth Heat Shield

All Dimensions in Inches

Fig. 8 Model and Sting Dimensions Used in Postflight Wind Tunnel Program

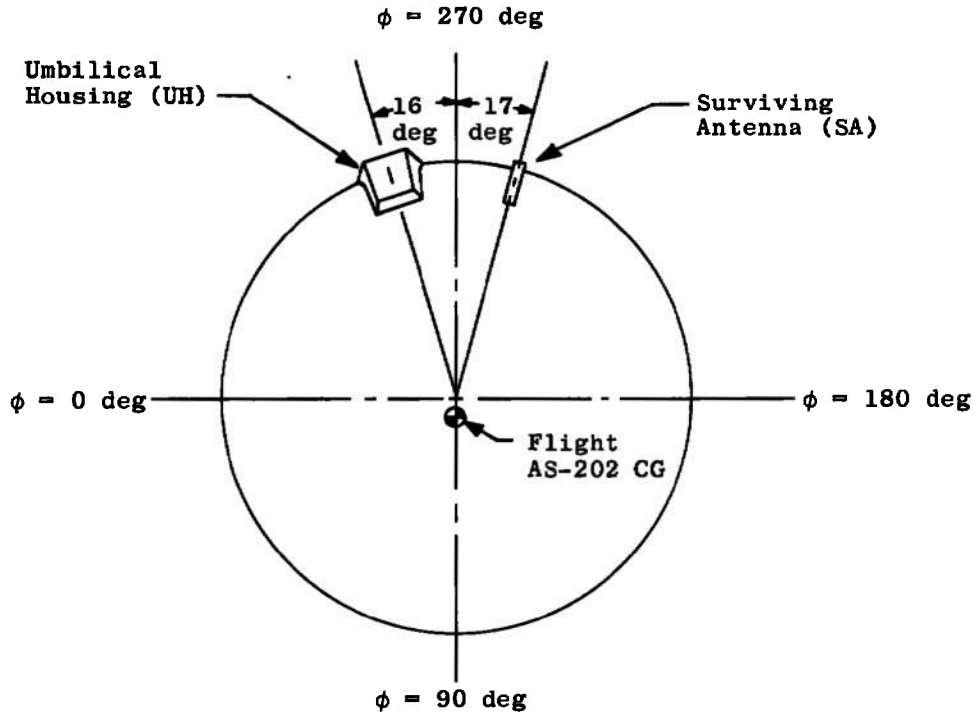

Tunnel	Heat Shield	Protuberances Used	Model Designation
A	Smooth	None	I
	Wavy	UH and SA	II
	Wavy	SA	III
B	Smooth	None	
	Wavy	UH and SA	
C	Smooth	None	
	Wavy	SA	
	Wavy	UH and SA	
F	Smooth	None	
	Wavy	UH	IV
G	Smooth	None	
L	Smooth	None	

a. Location of Protuberances

Fig. 9 Model External Protuberances

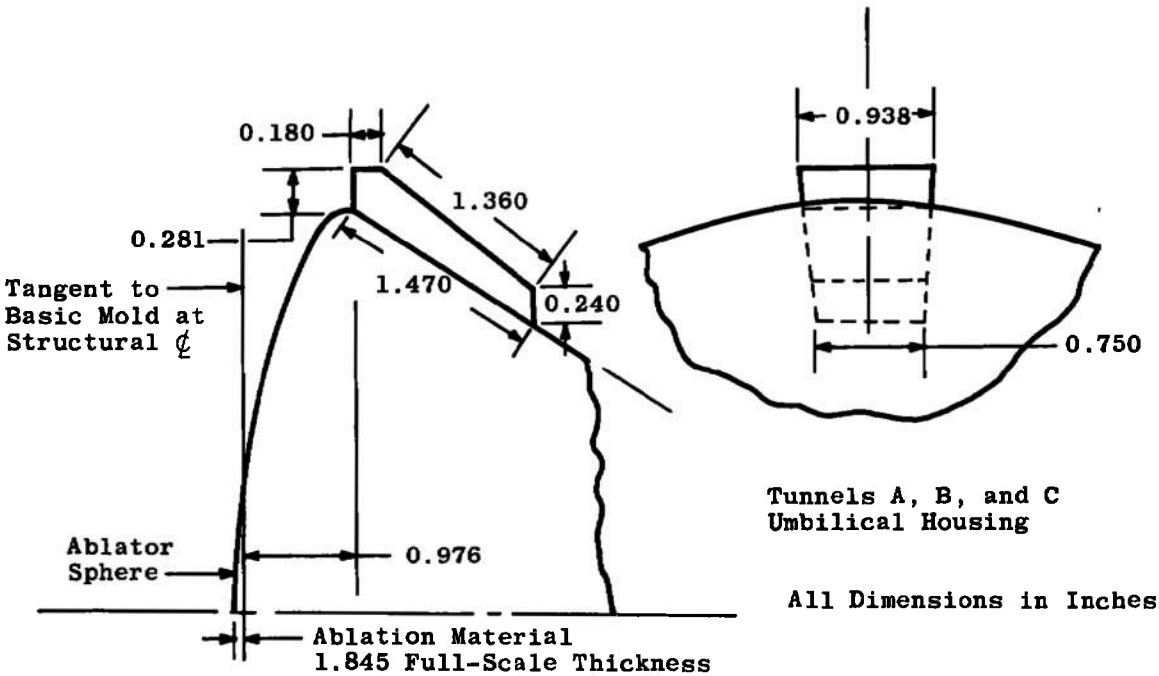

x	y
0	0
0	0.115
0.012	0.203
0.051	0.255
0.153	0.353
0.305	0.407
0.407	0.415
0.509	0.407
0.661	0.366
0.814	0.251
0.865	0.180
0.915	0.069
0.938	0

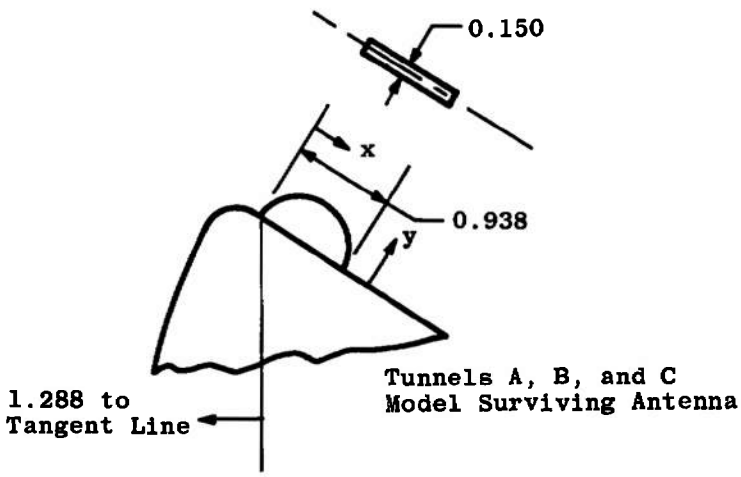

b. Protuberances Details - Tunnel A, B, and C Model

Fig. 9 Concluded

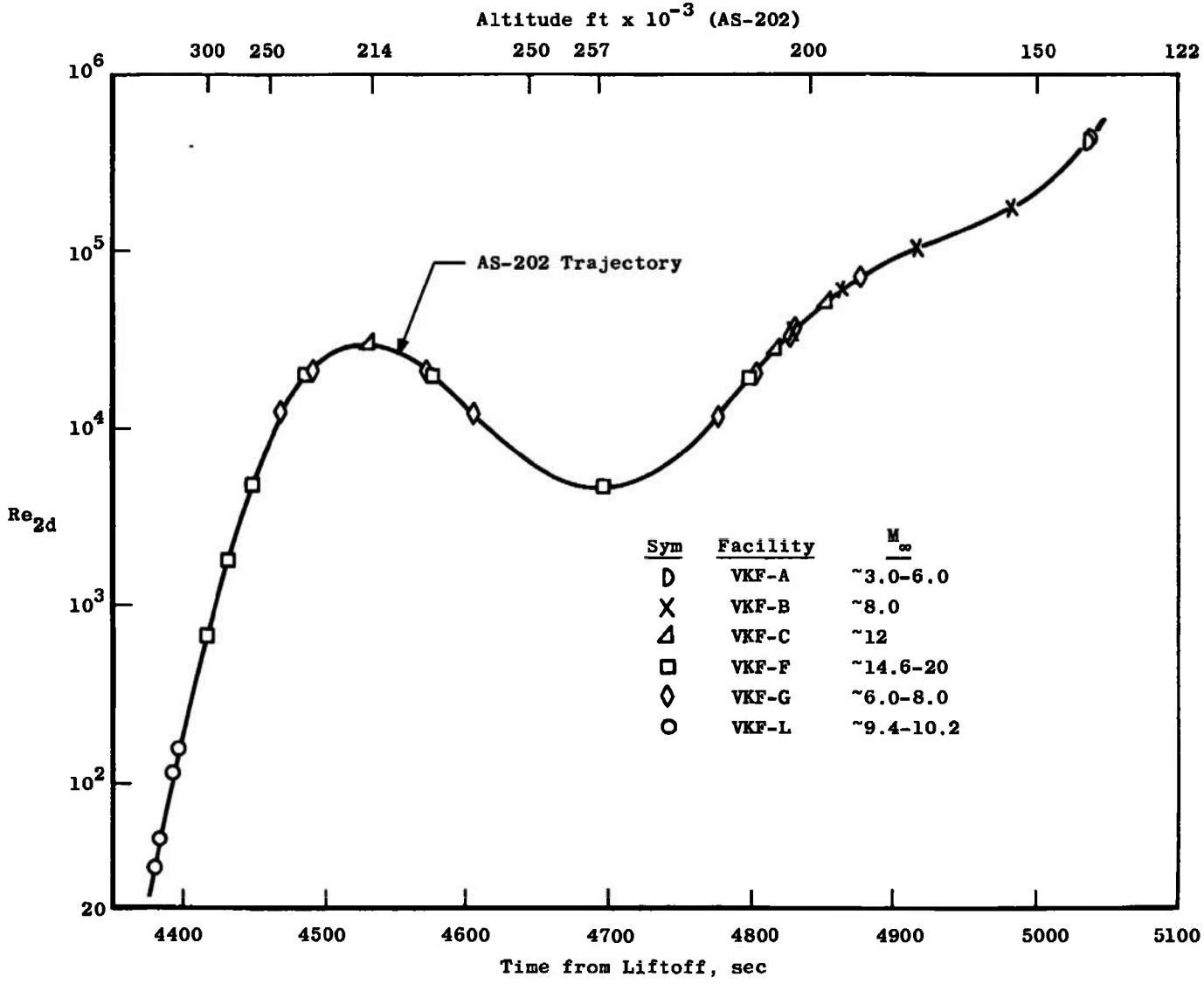

Fig. 10 Shock Reynolds Number Flight Simulation

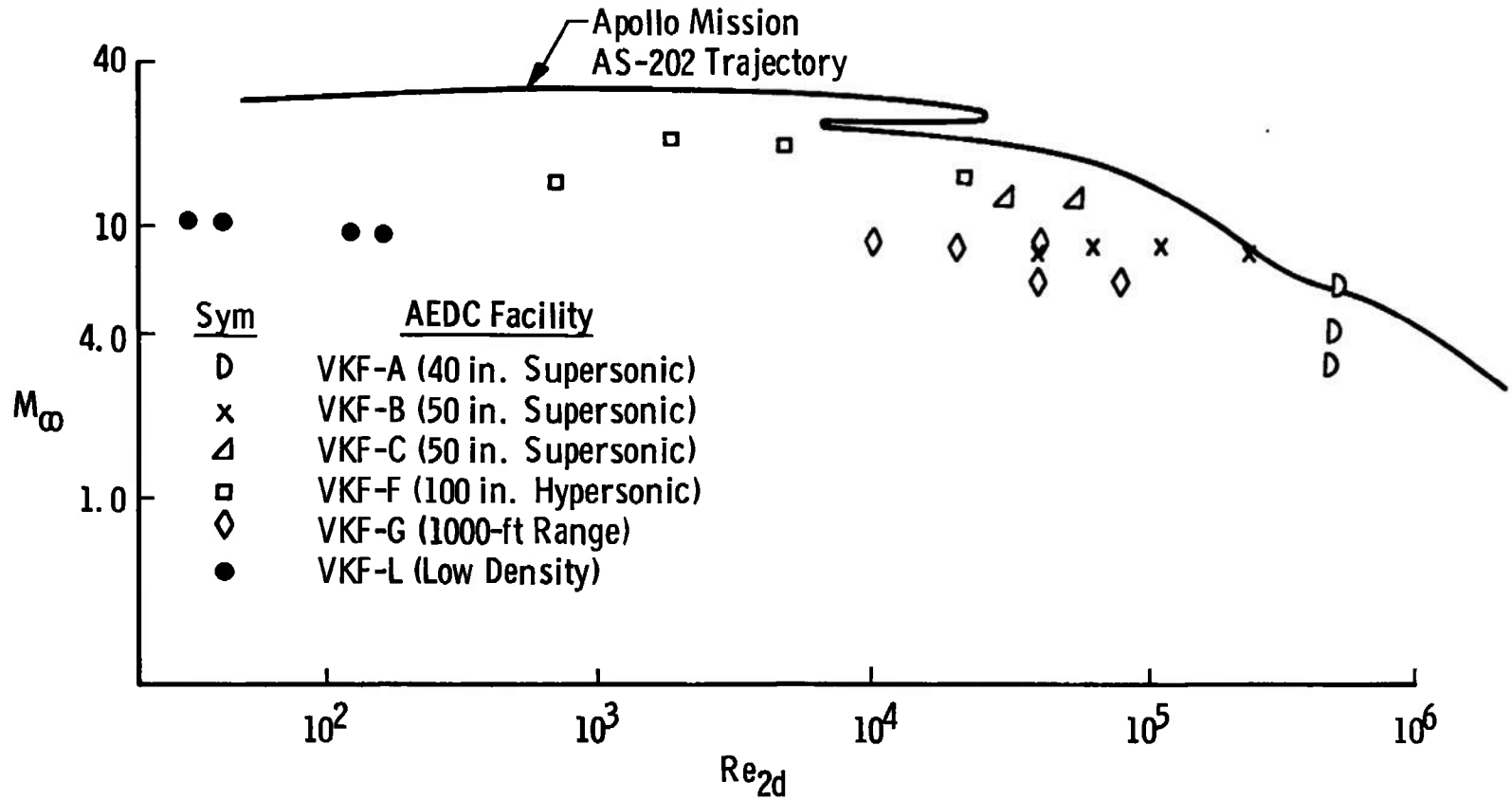

Fig. 11 Mach Number and Shock Reynolds Number Flight Simulation

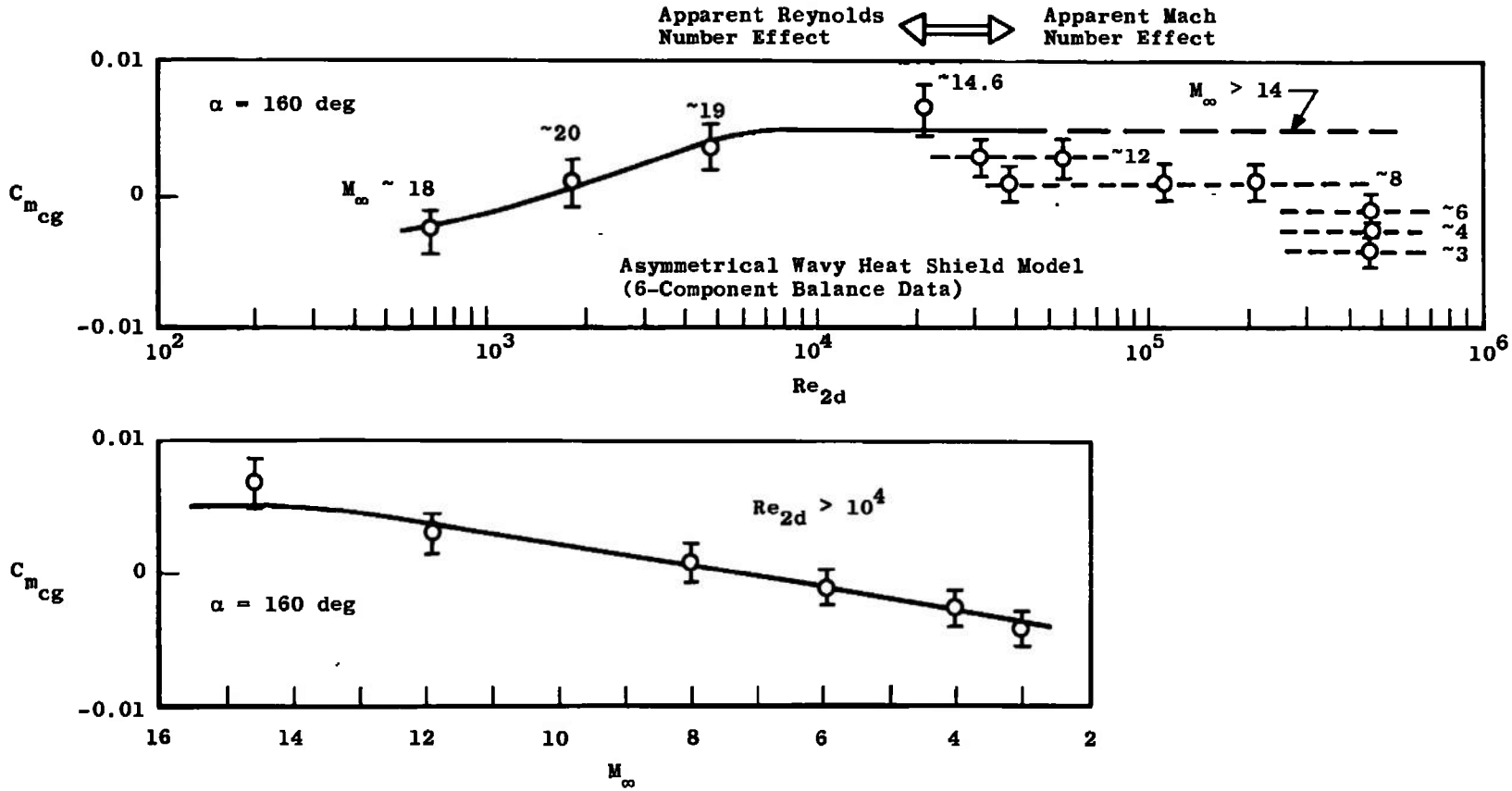

Fig. 12 Typical Data Plot Showing Basis of Data Correlation

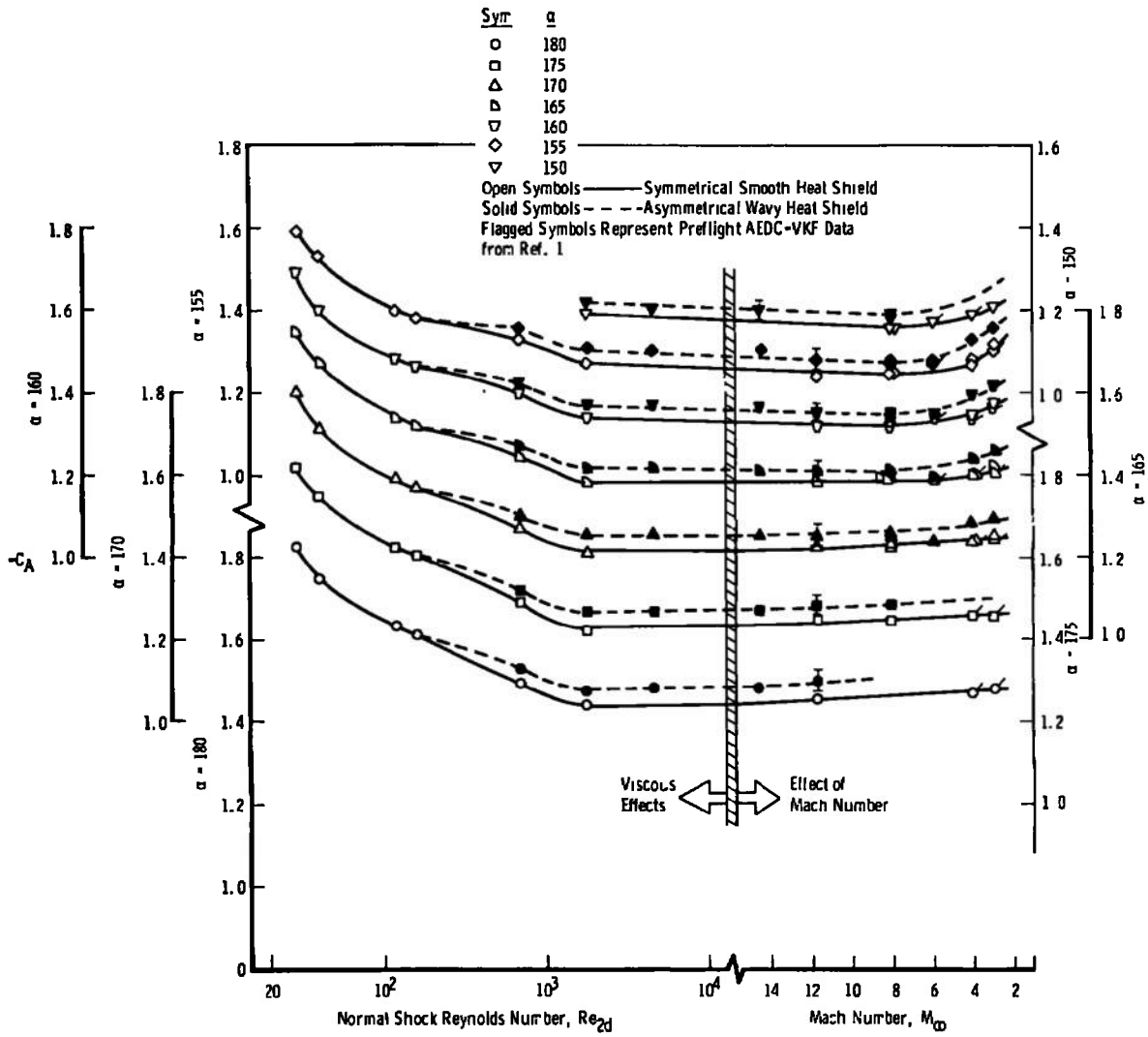

Fig. 13 Variation of Axial-Force Coefficient (C_A) with M_∞ and Re_{2d}

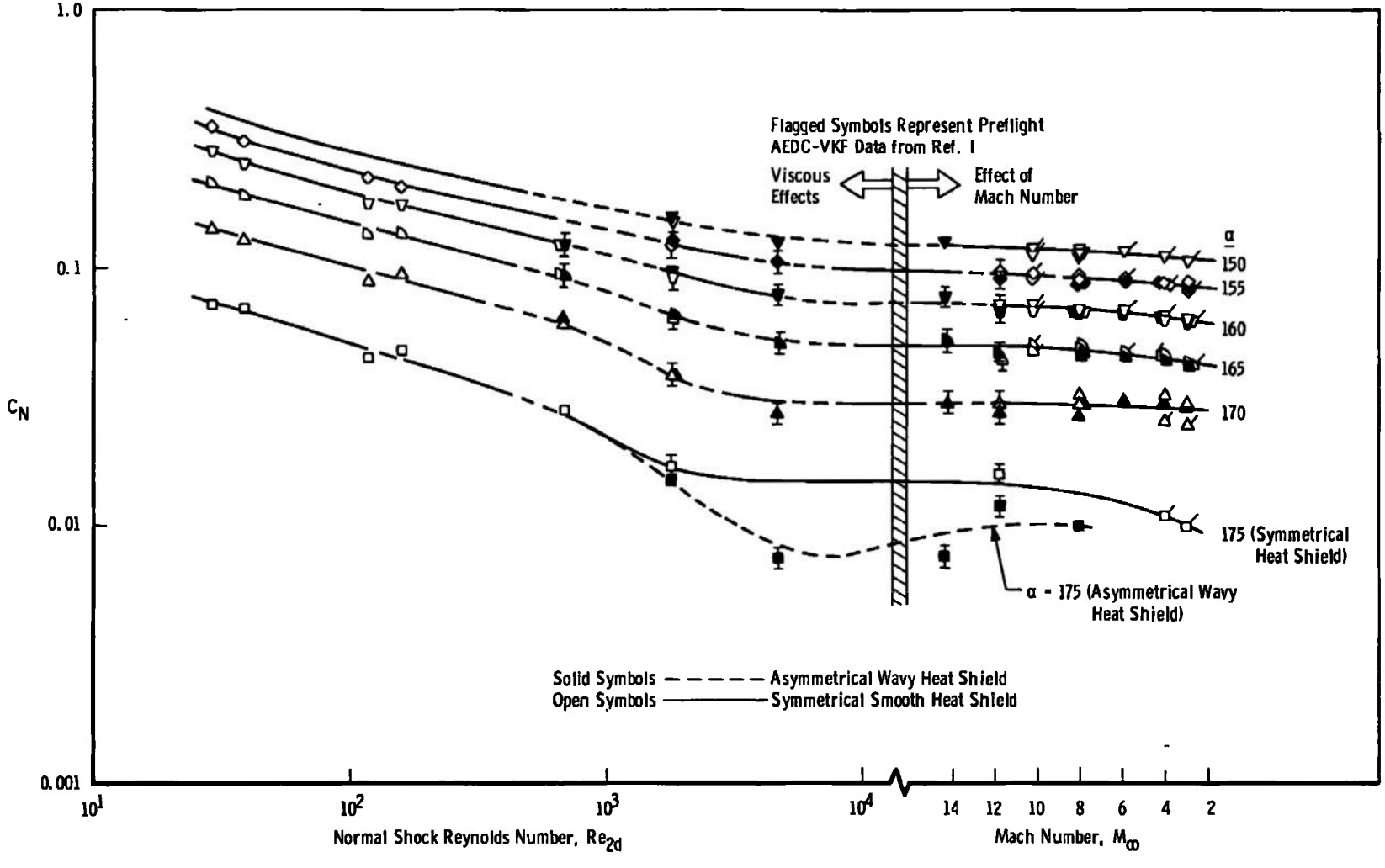

Fig. 14 Variation of Normal-Force Coefficient (C_N) with M_∞ and Re_{2d}

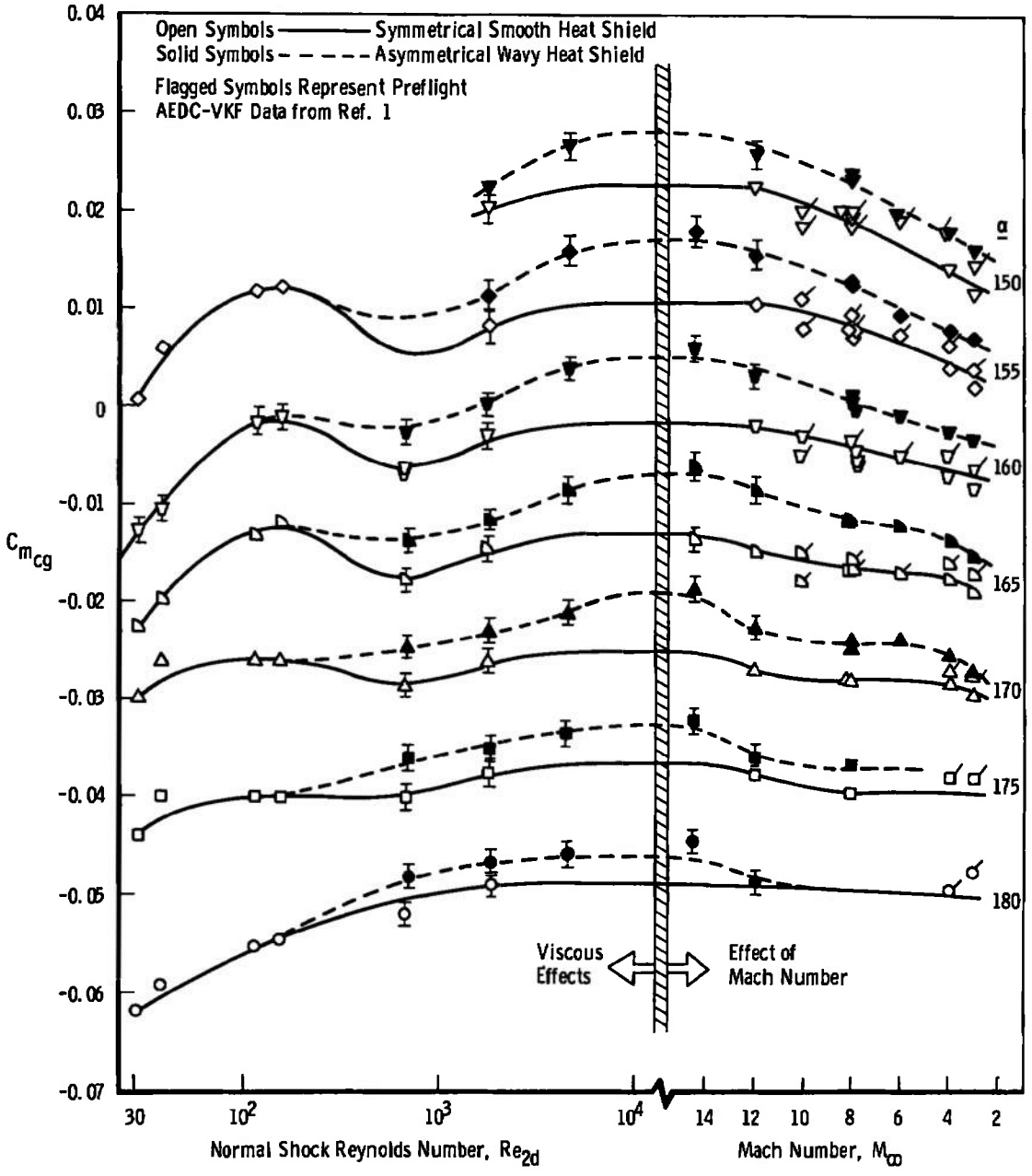

Fig. 15 Variation of Pitching-Moment Coefficient (Cm_{cg}) with M_∞ and Re_{2d}

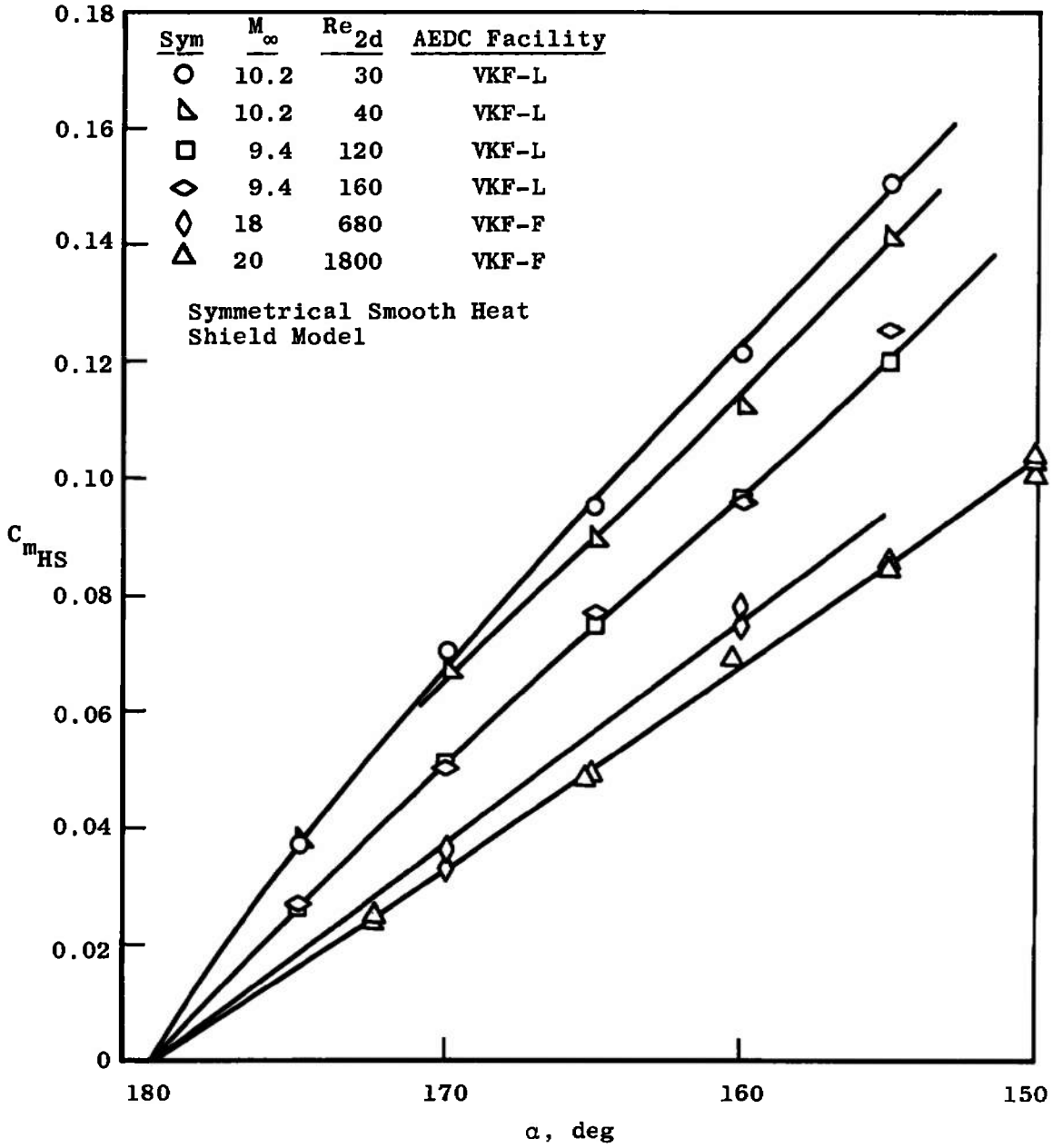

Fig. 16 Variation of Pitching Moment Referenced to Heat Shield (Cm_{HS}) with Re_{2d}

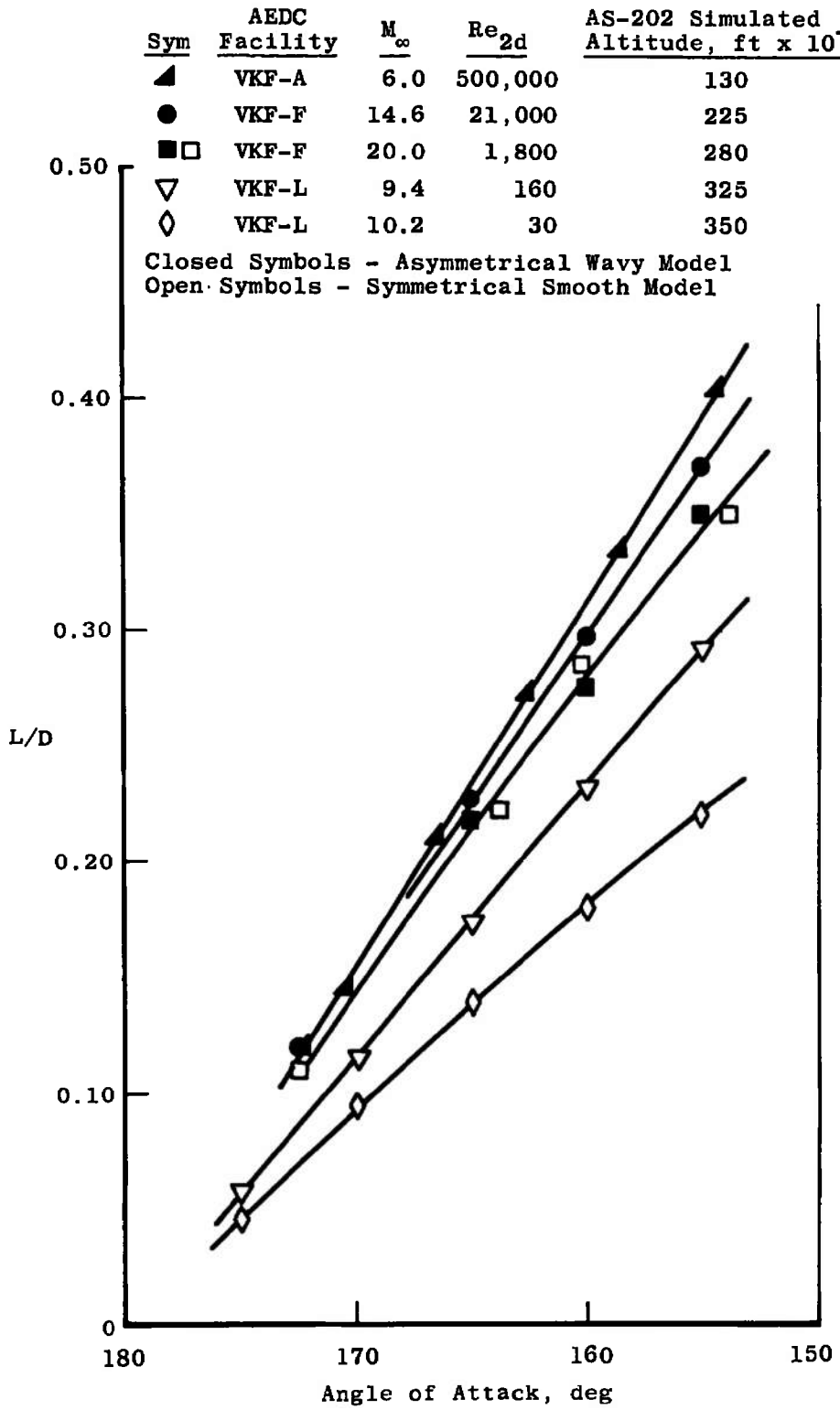

Fig. 17 Effect of Shock Reynolds Number on Lift-to-Drag Ratio

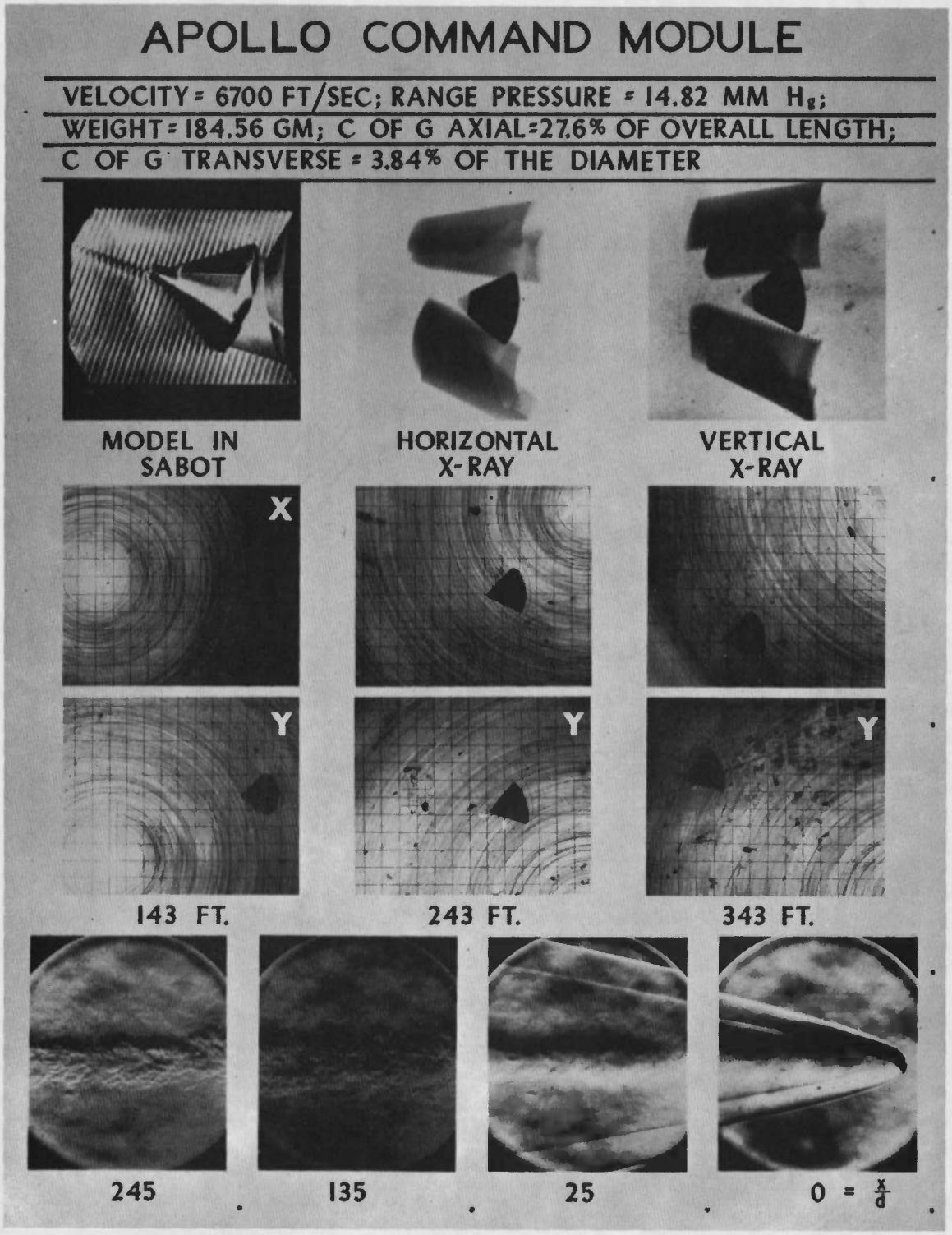

Fig. 18 Photographic History of Range G Shot

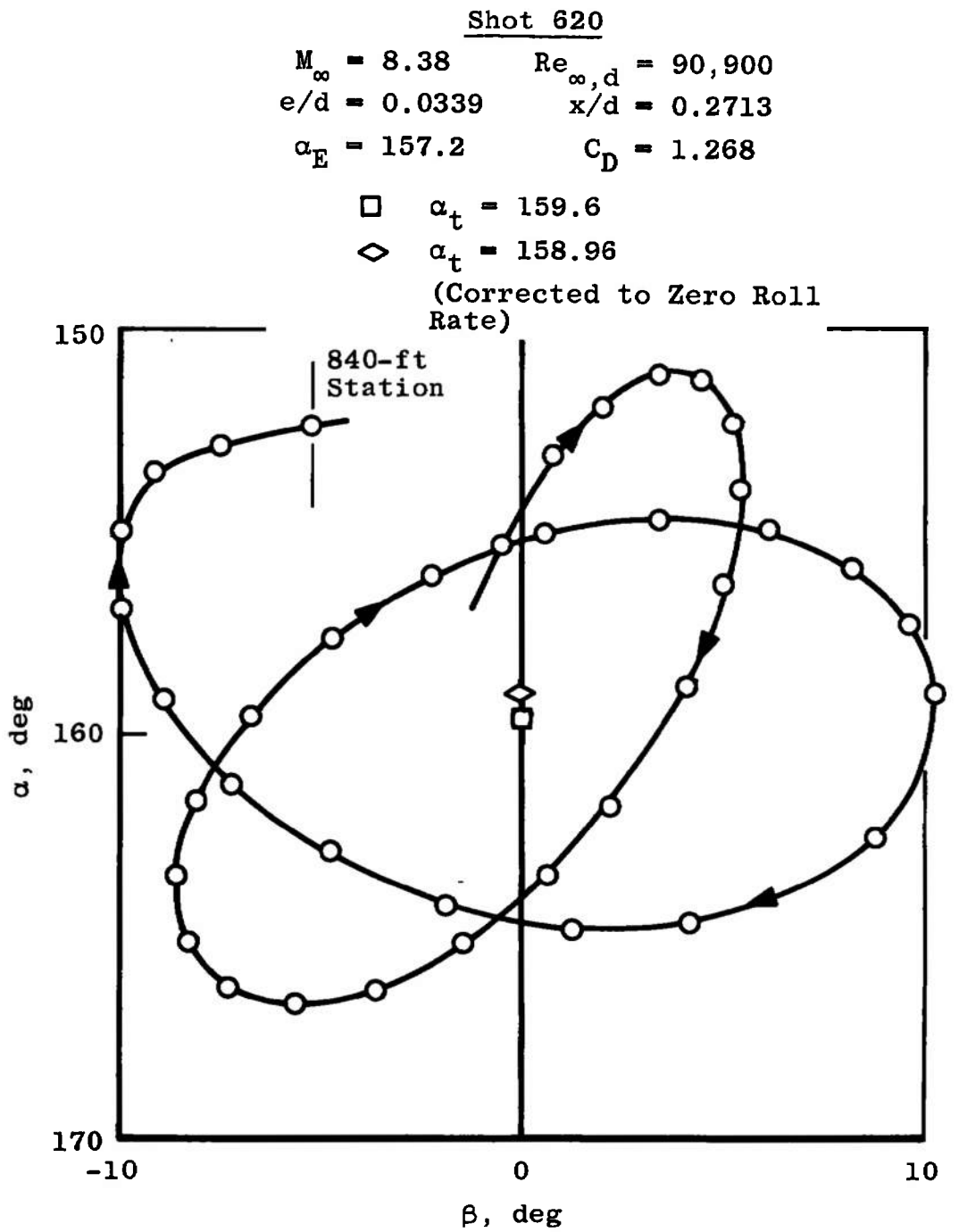

a. Variation of α and β (Body Angles)

Fig. 19 Flight of Apollo Model in Range G, Shot 620

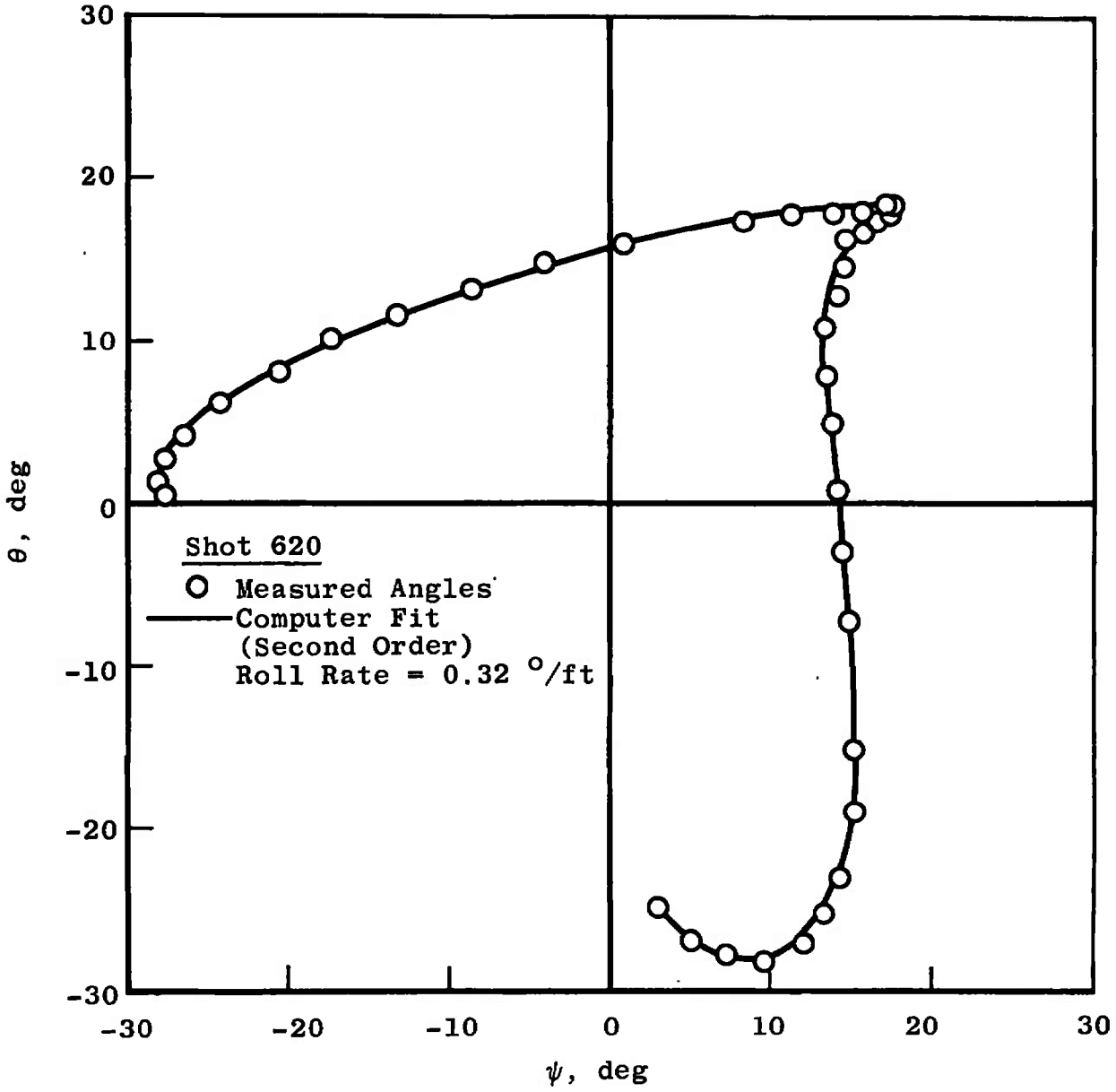

b. Variation of θ and ψ (Range Angles)

Fig. 19 Concluded

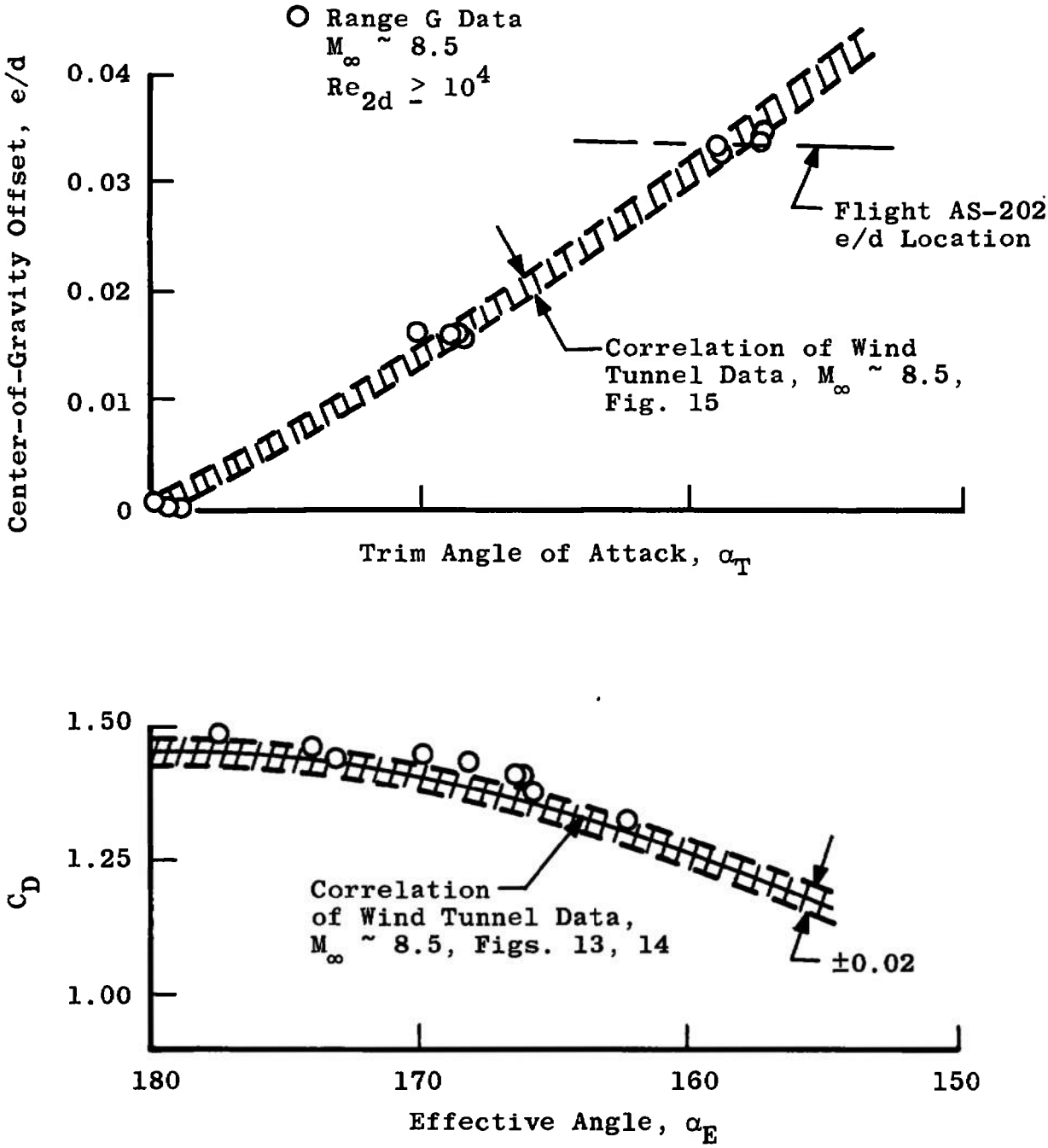

Fig. 20 Comparison of Free-Flight (AEDC-Range G) to Sting Mounted Tunnel Data

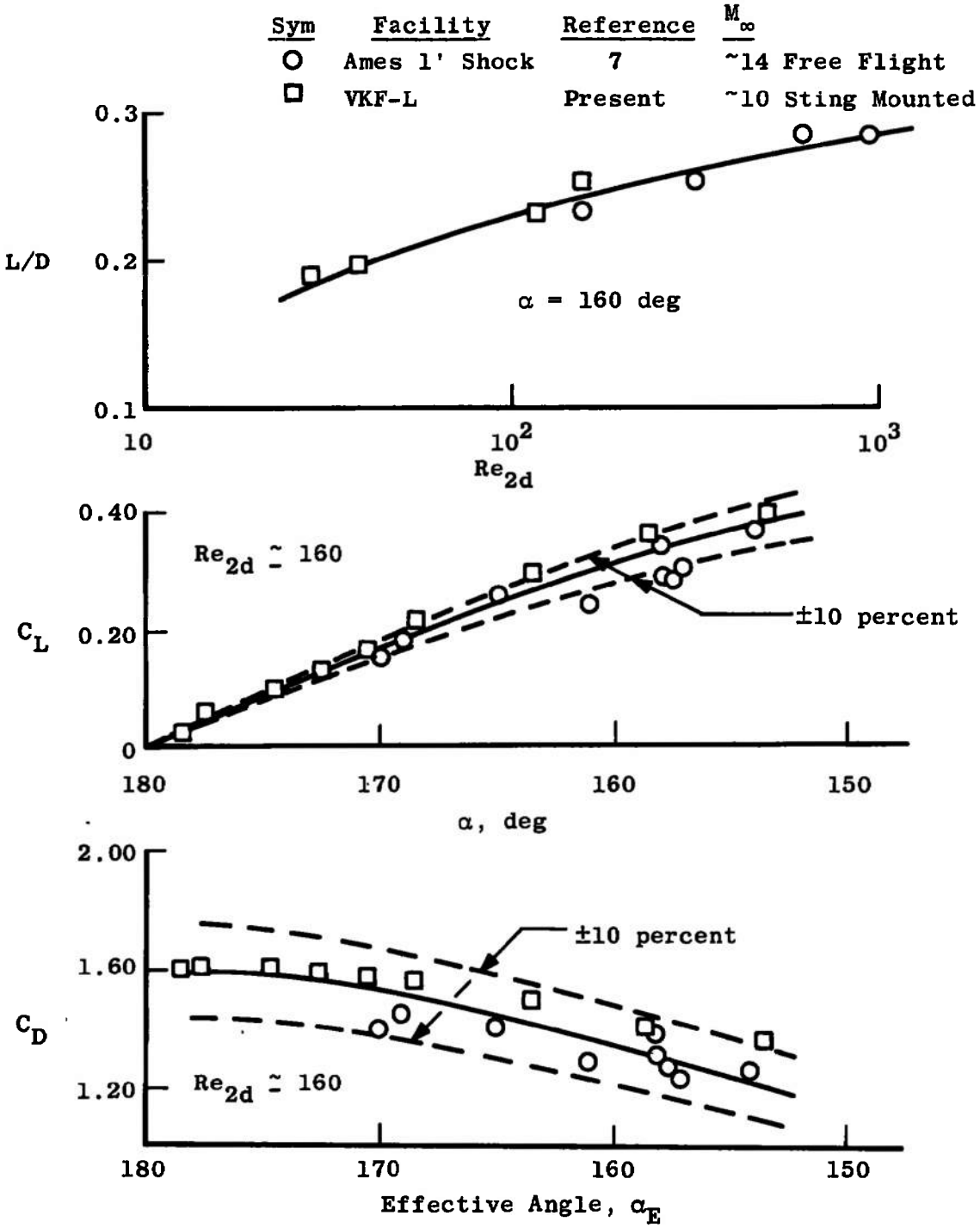

Fig. 21 Comparison of Free-Flight (Ames Shock Tunnel) to Sting Mounted Tunnel Data

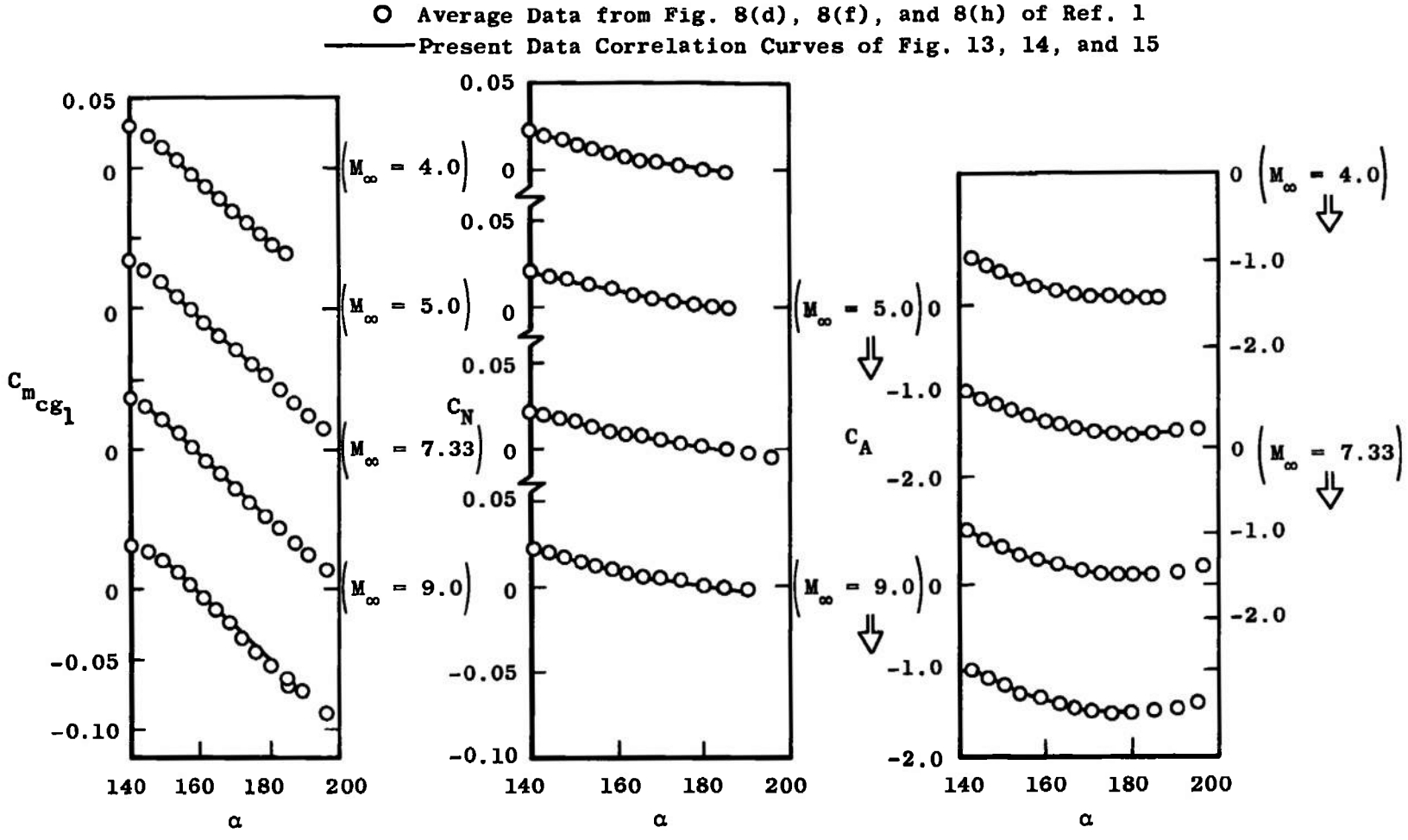

Fig. 22 Comparison of Present Results with Previous Data, Symmetrical Smooth Heat Shield

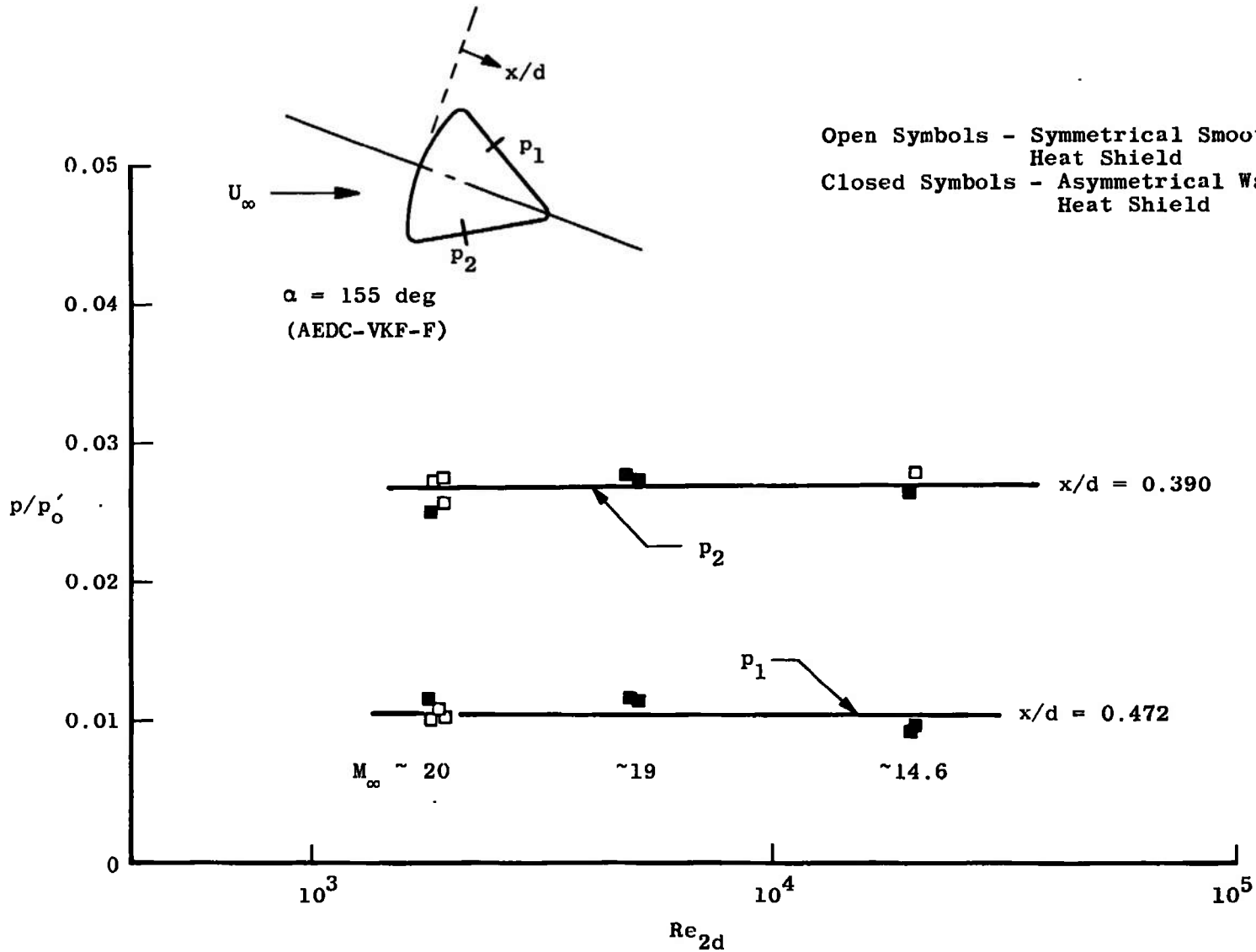

Fig. 23 Variation of Afterbody Pressures with Reynolds Number, $M_\infty > 14$

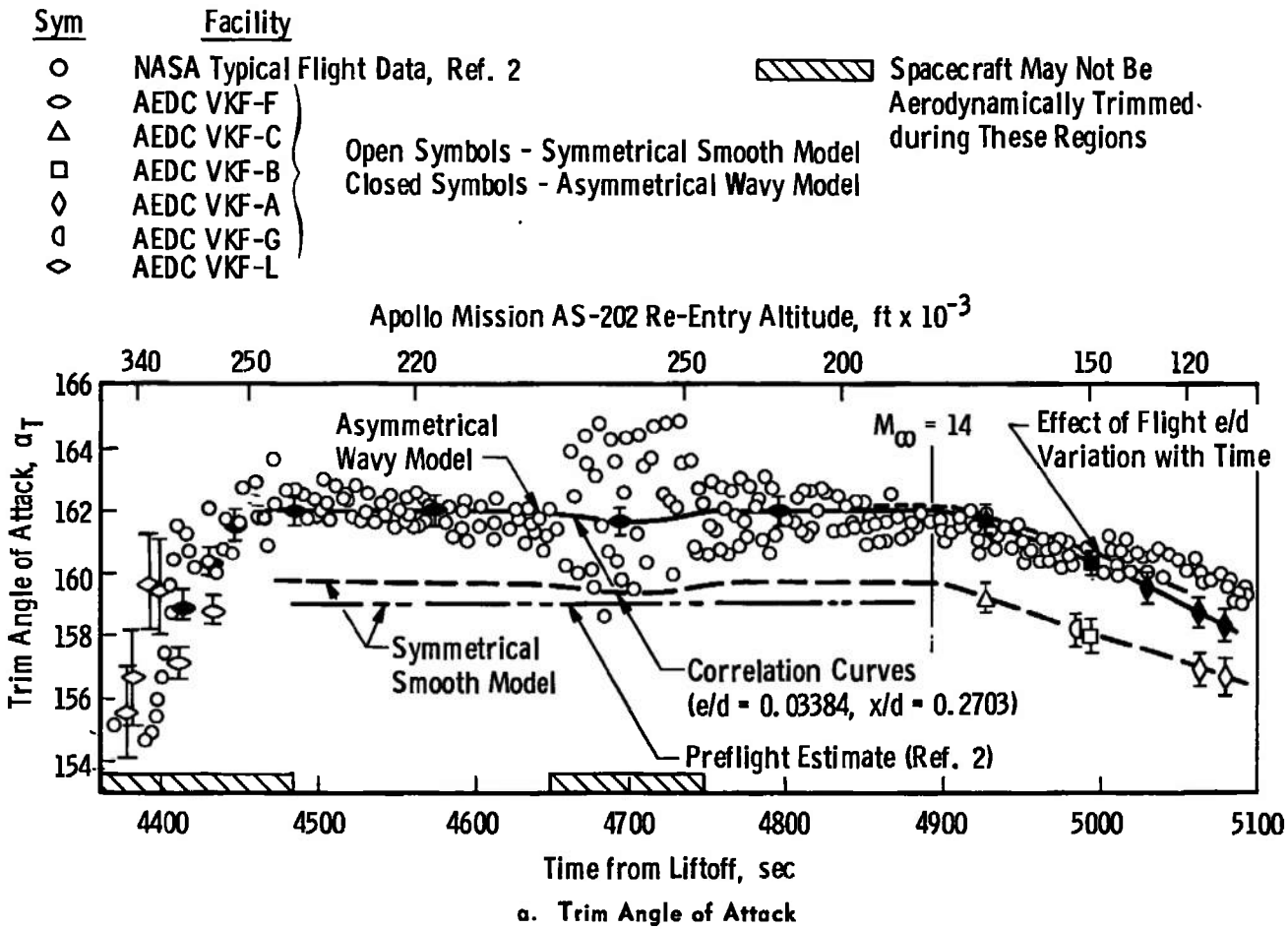

a. Trim Angle of Attack

Fig. 24 Comparison of Apollo Mission AS-202 Flight Data with AEDC-VKF Tunnel Data

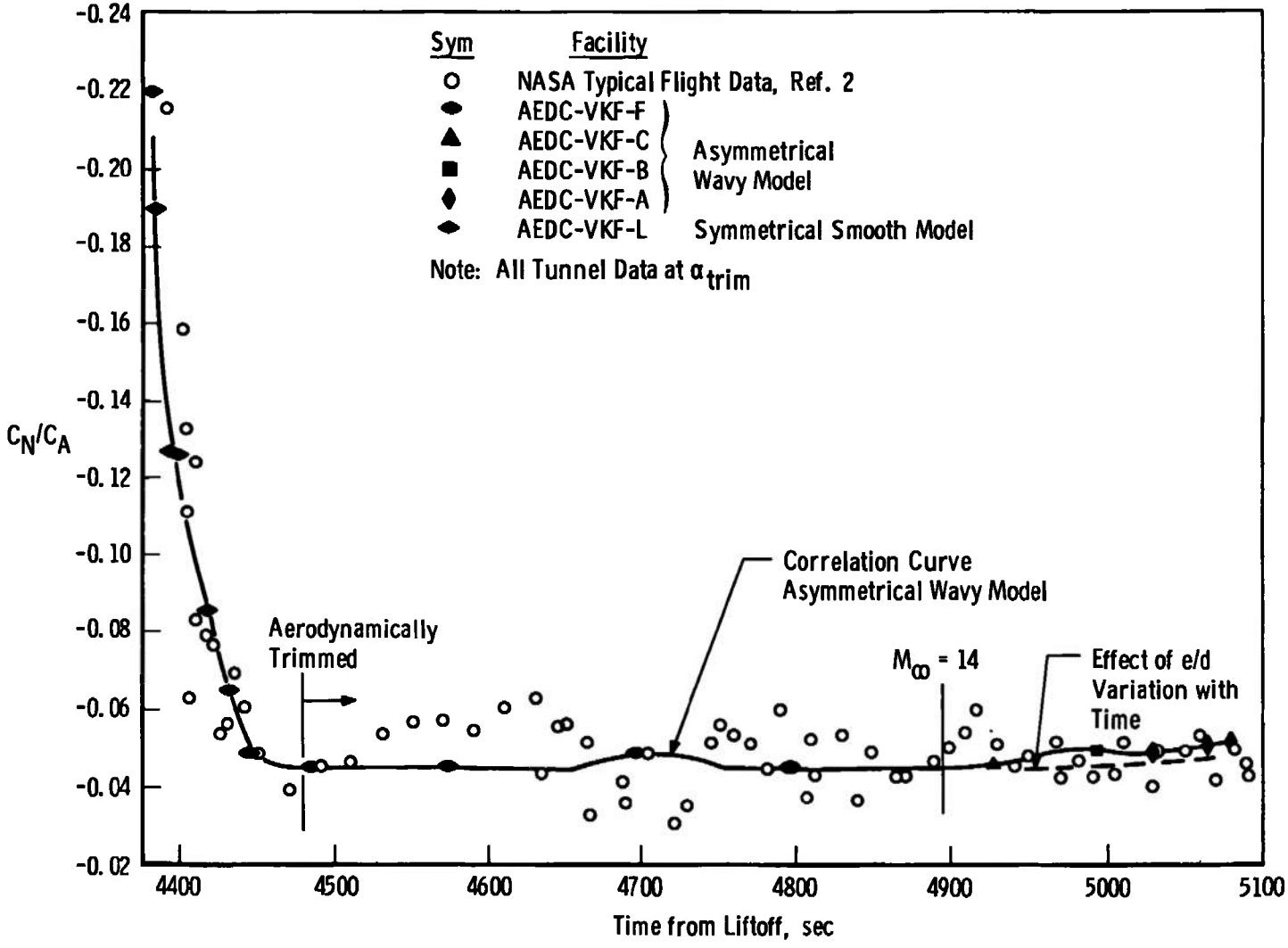

b. Normal to Axial-Force Ratio

Fig. 24 Continued

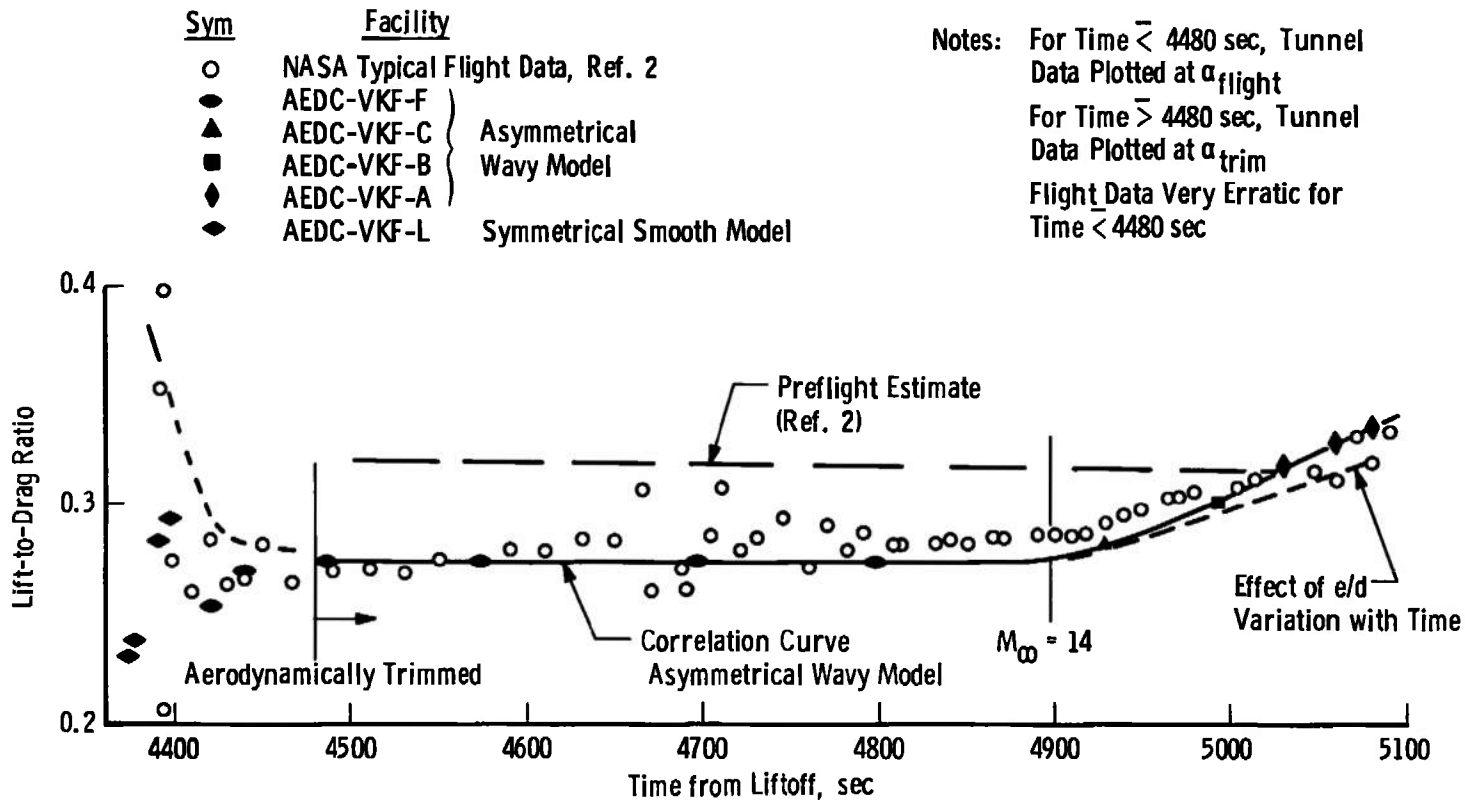

c. Lift to Drag Ratio

Fig. 24 Concluded

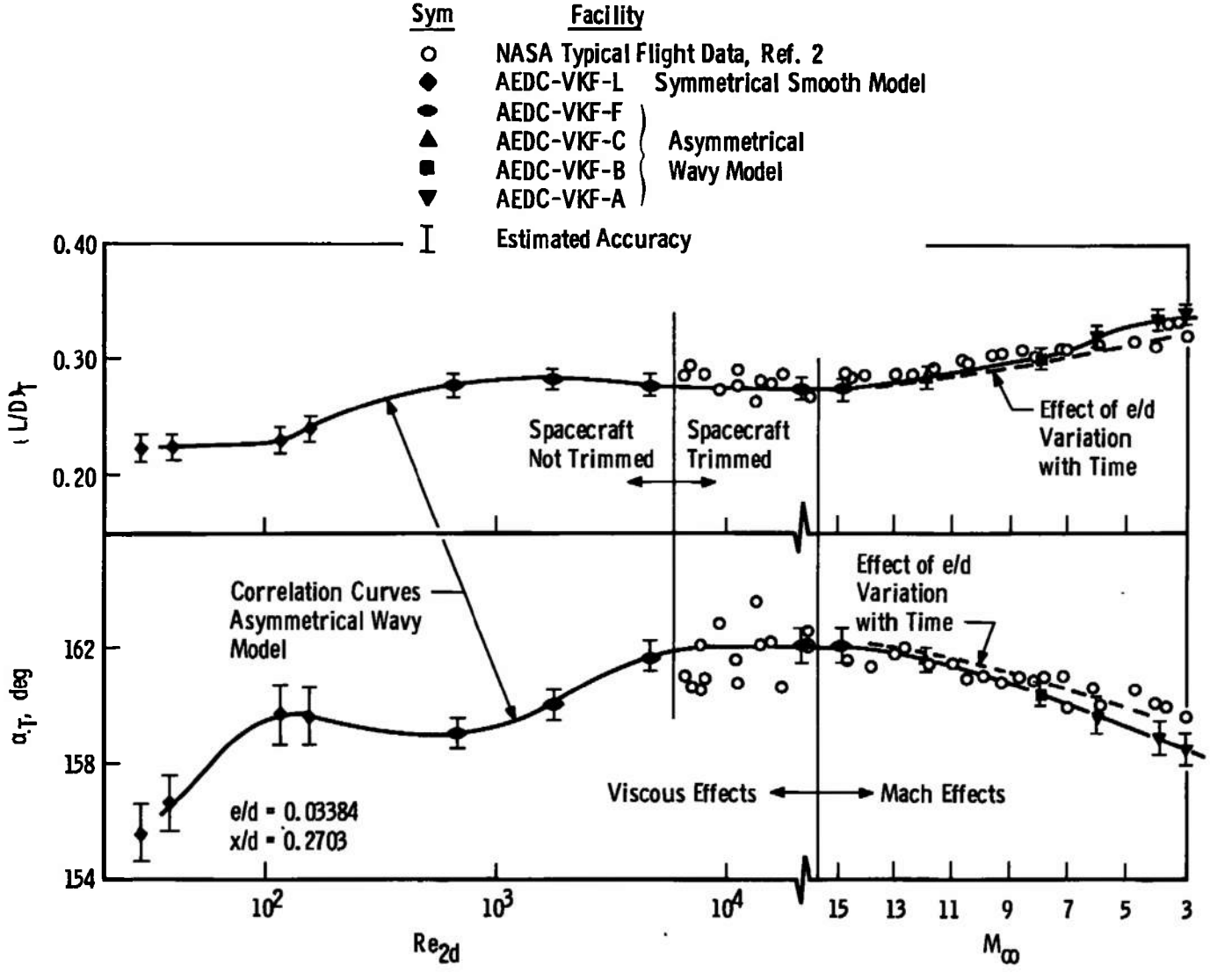

Fig. 25 Summary of $(L/D)_T$ and α_T Data

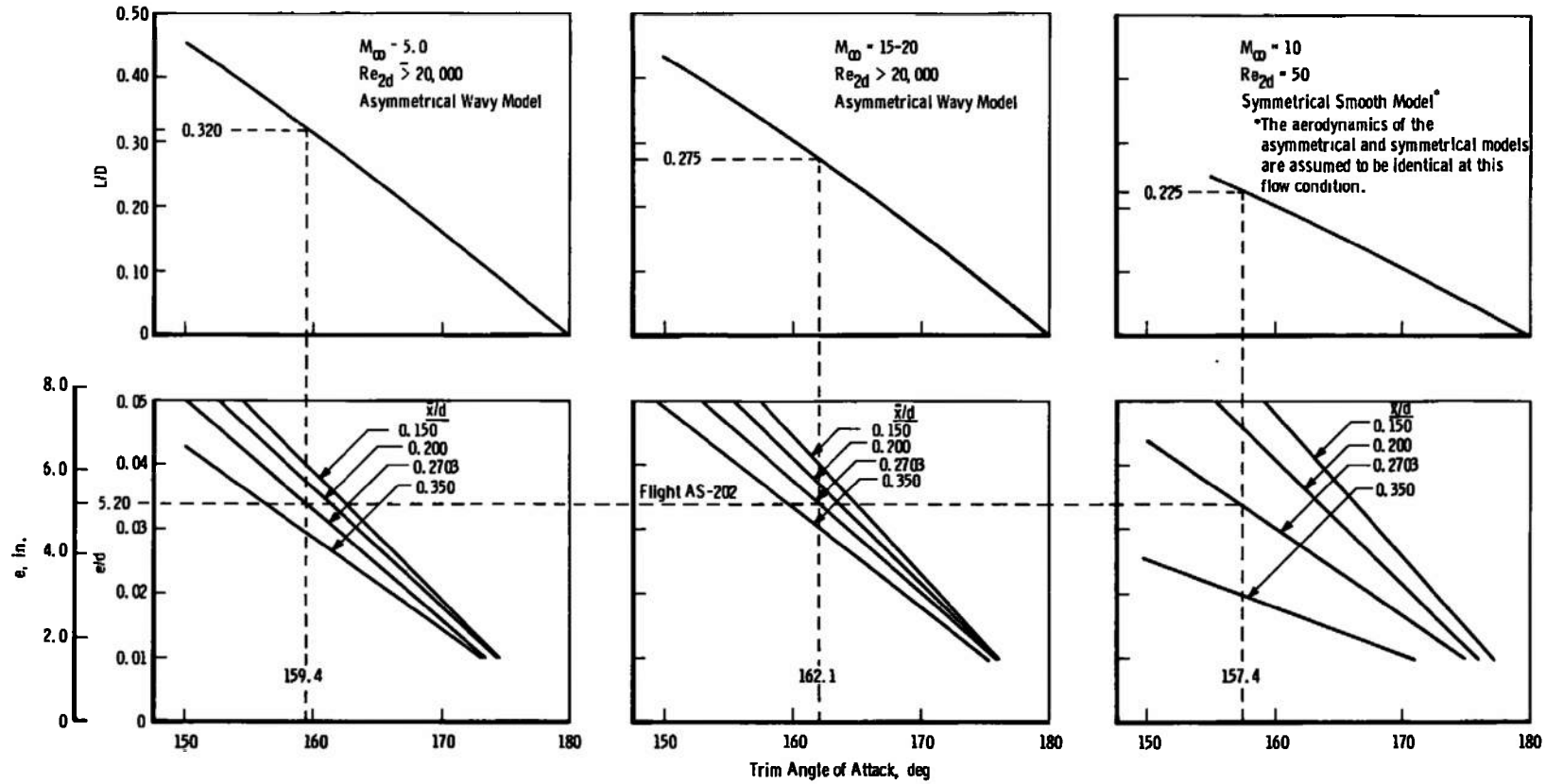

Fig. 26 Effect of Center-of-Gravity Location at Three Flow Conditions

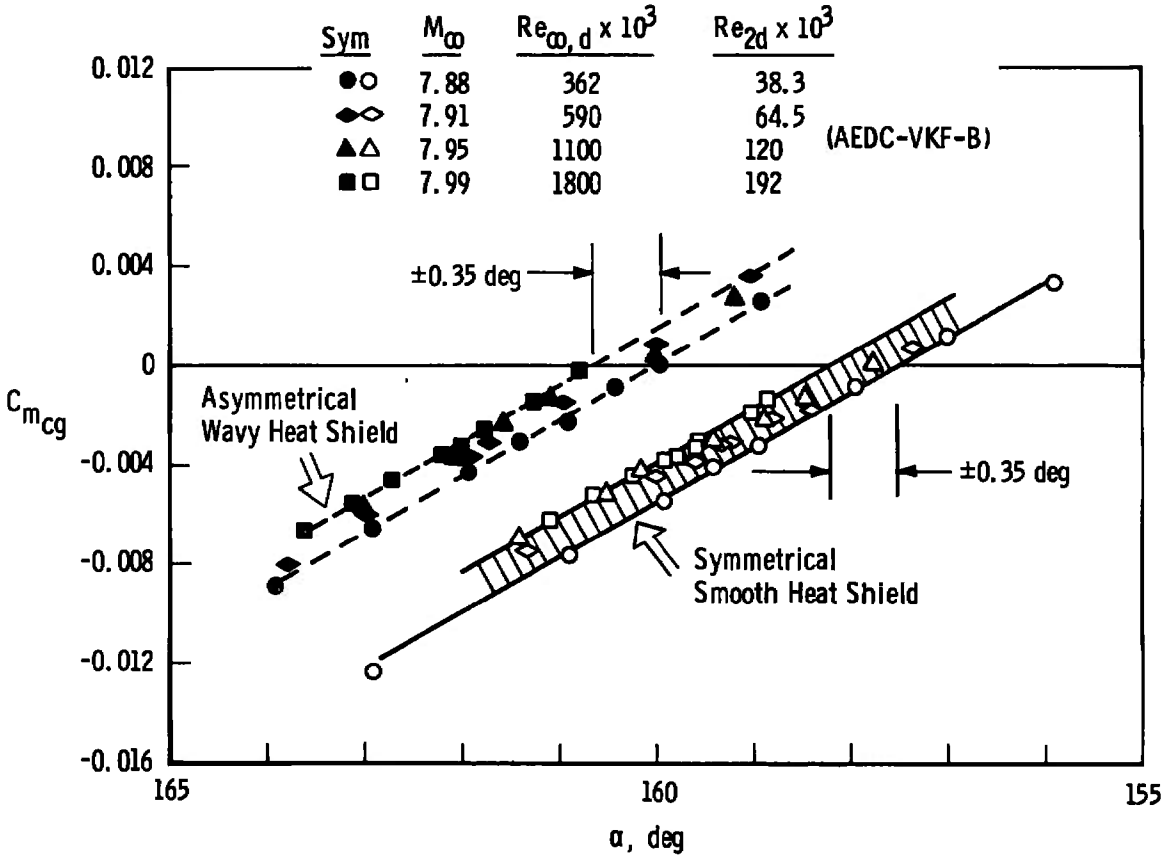

o. Data from Free Oscillation, Cross-Flexure Pivot Balance

Fig. II-1 Basic Wind Tunnel Data Showing Effect of Heat Shield

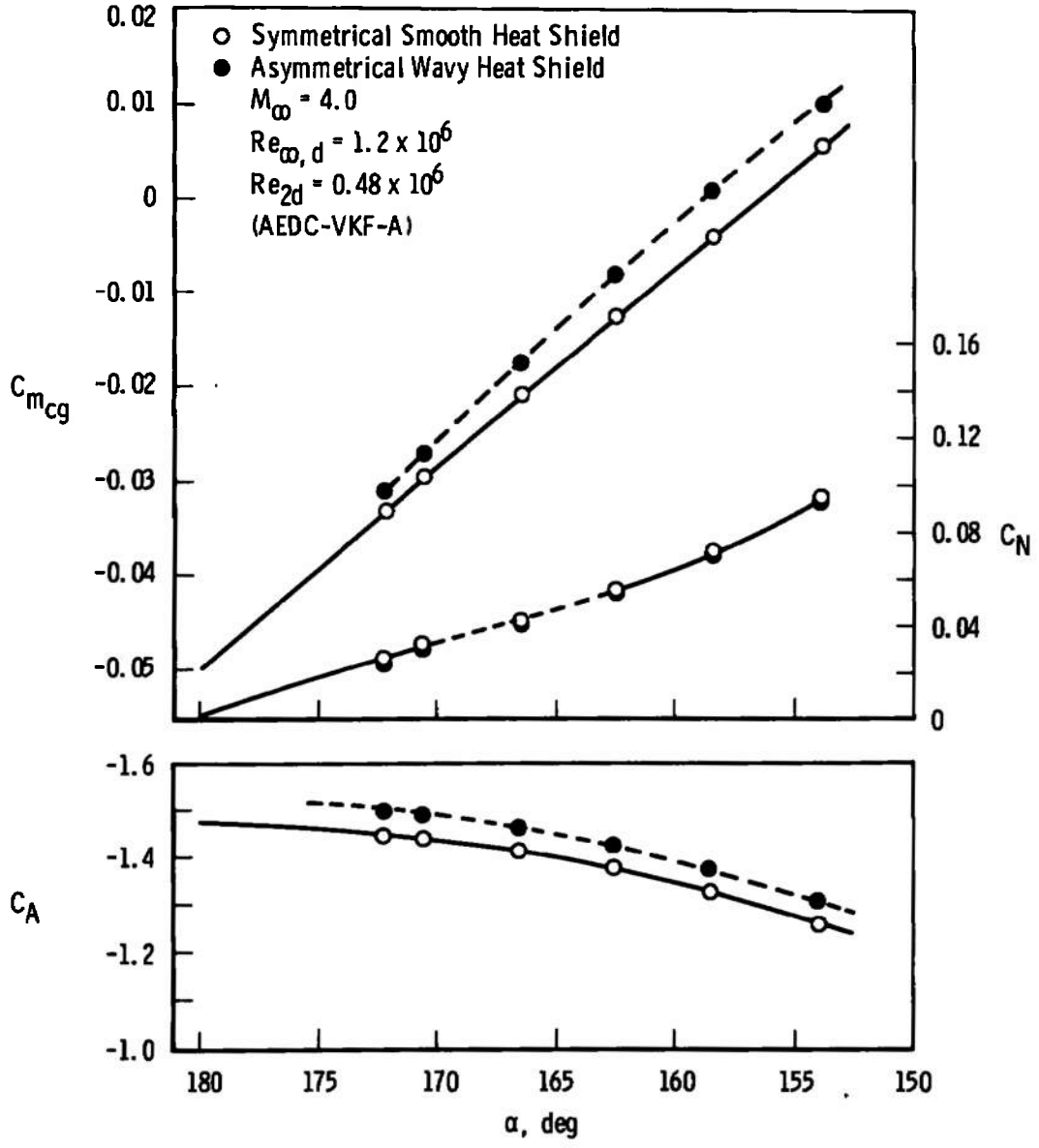

b. Six-Component Balance Data, M_∞ = 4.0

Fig. II-1 Continued

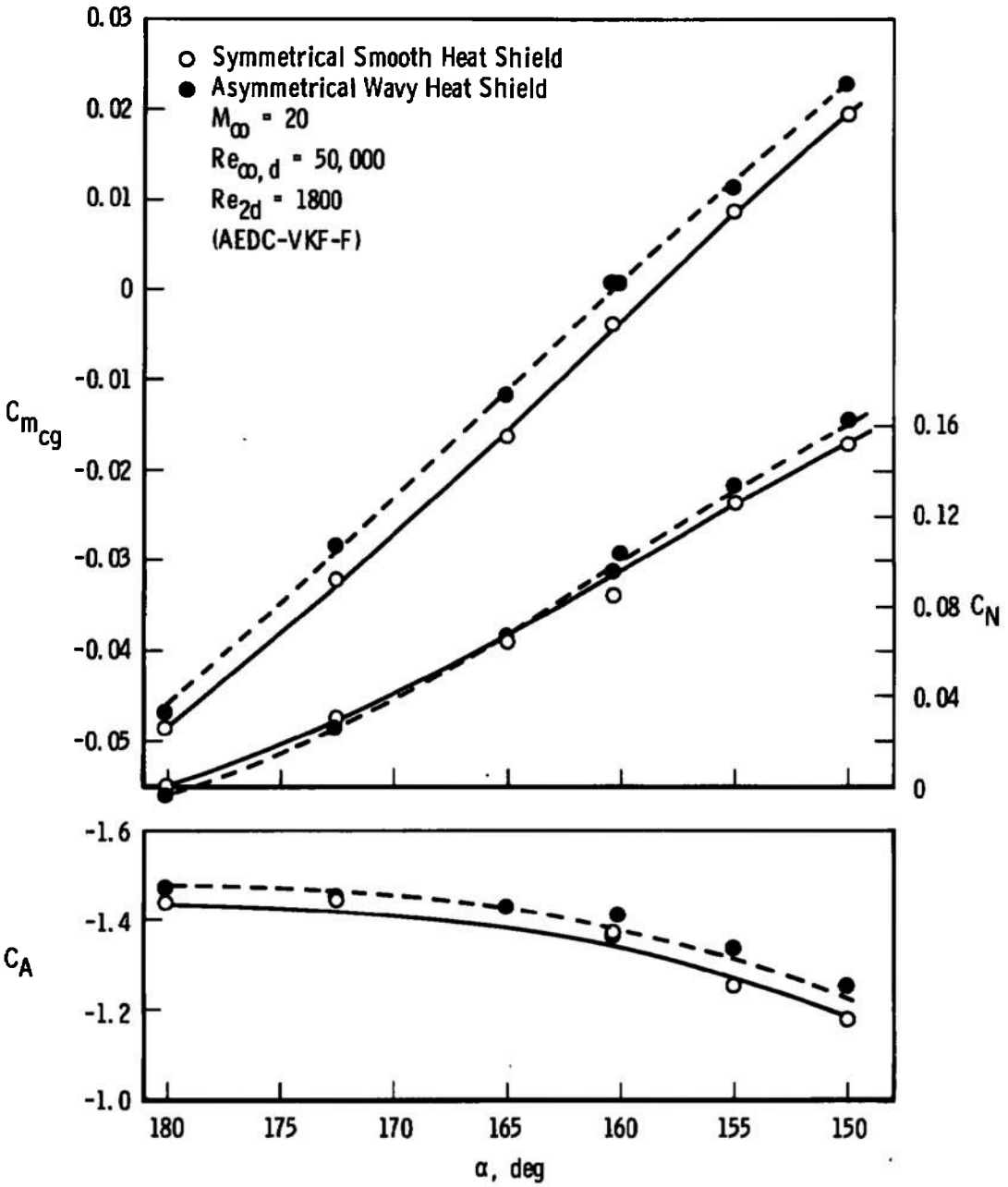

c. Six-Component Balance Data, M_∞ = 20

Fig. II-1 Concluded

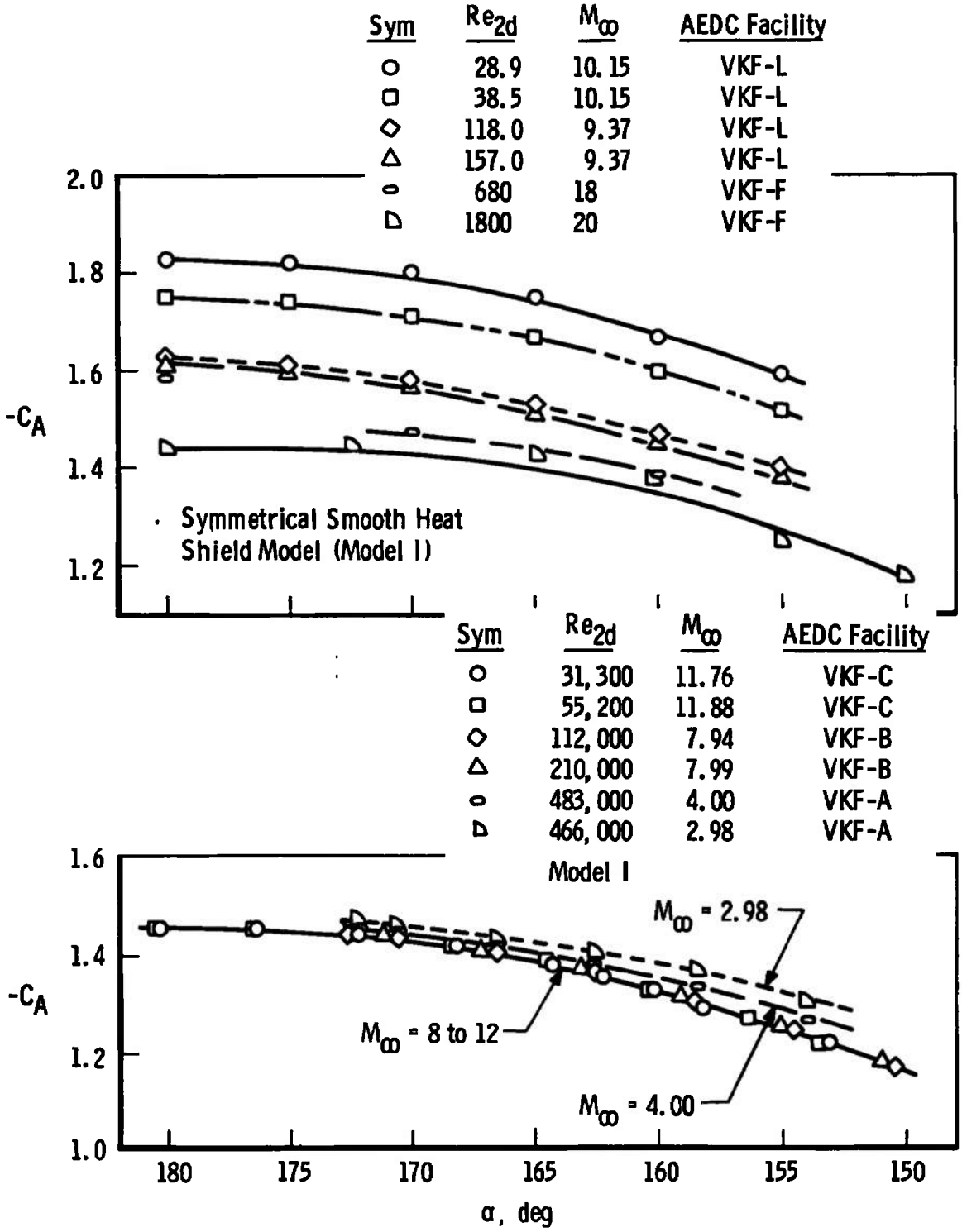

a. Variation of C_A with α, Symmetrical Model

Fig. II-2 Variation of Aerodynamic Forces with Re_{2d}, Basic Data

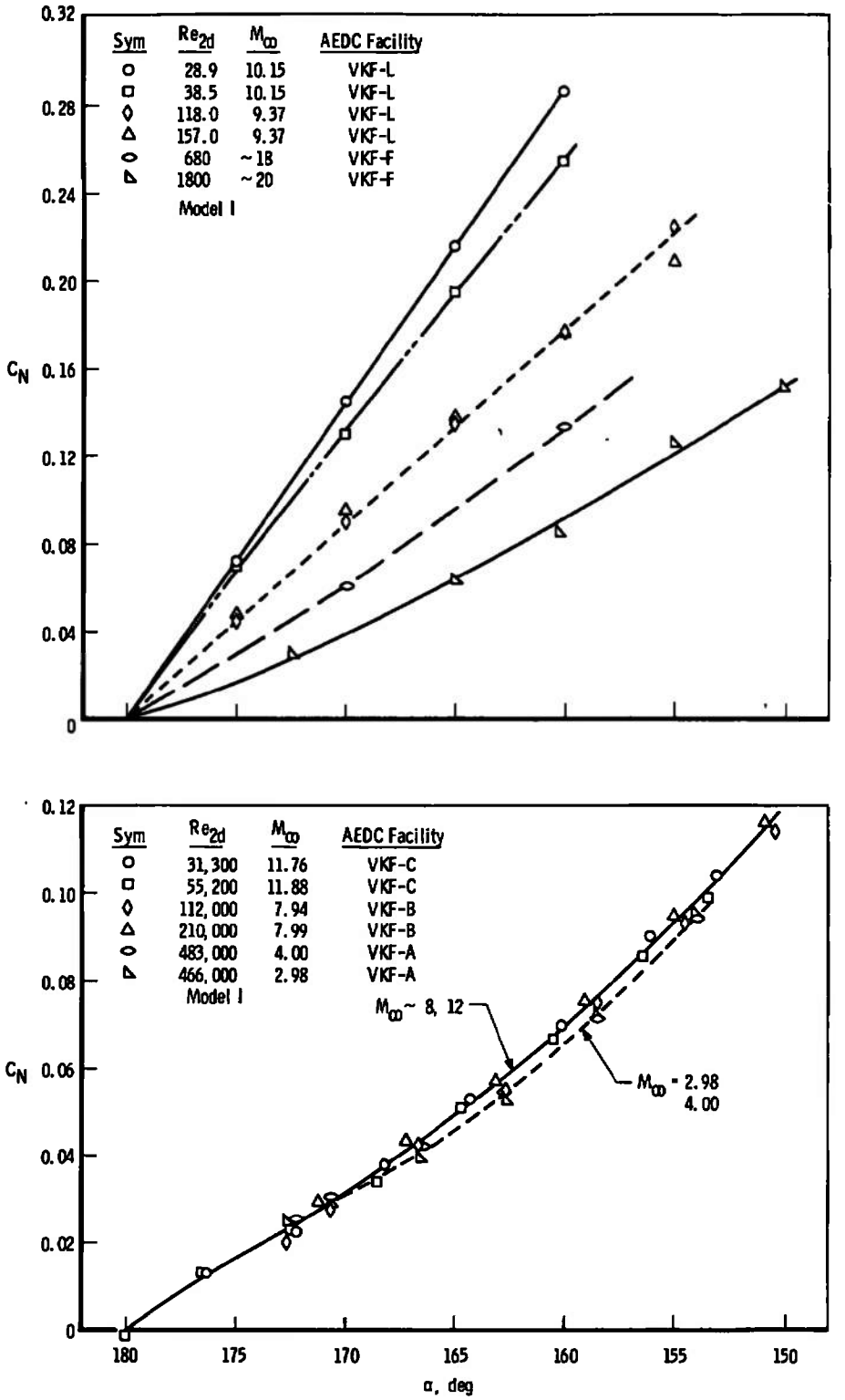

b. Variation of C_N with α, Symmetrical Model

Fig. II-2 Continued

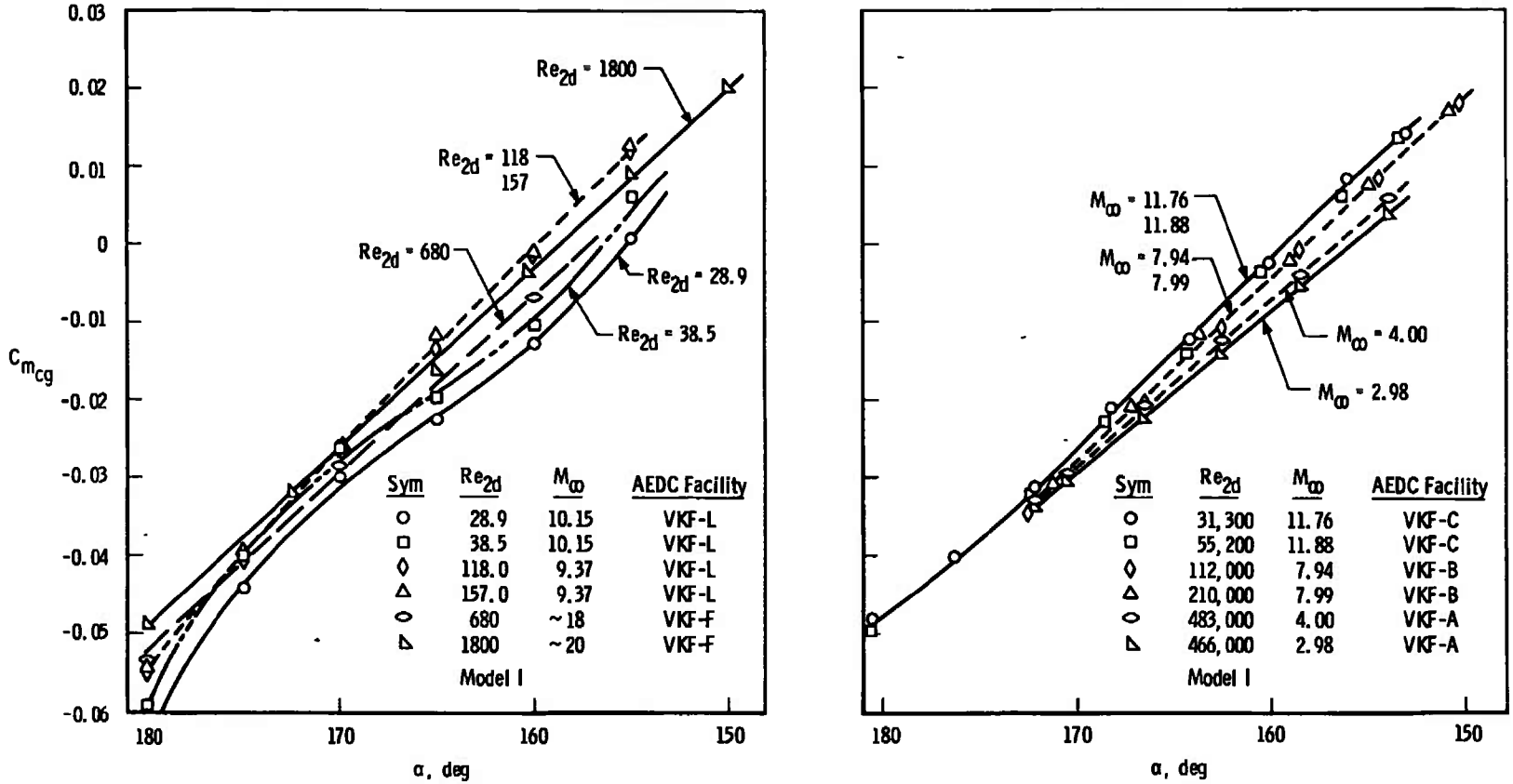

c. Variation of $C_{m_{cg}}$ with α, Symmetrical Smooth Model

Fig. II-2 Continued

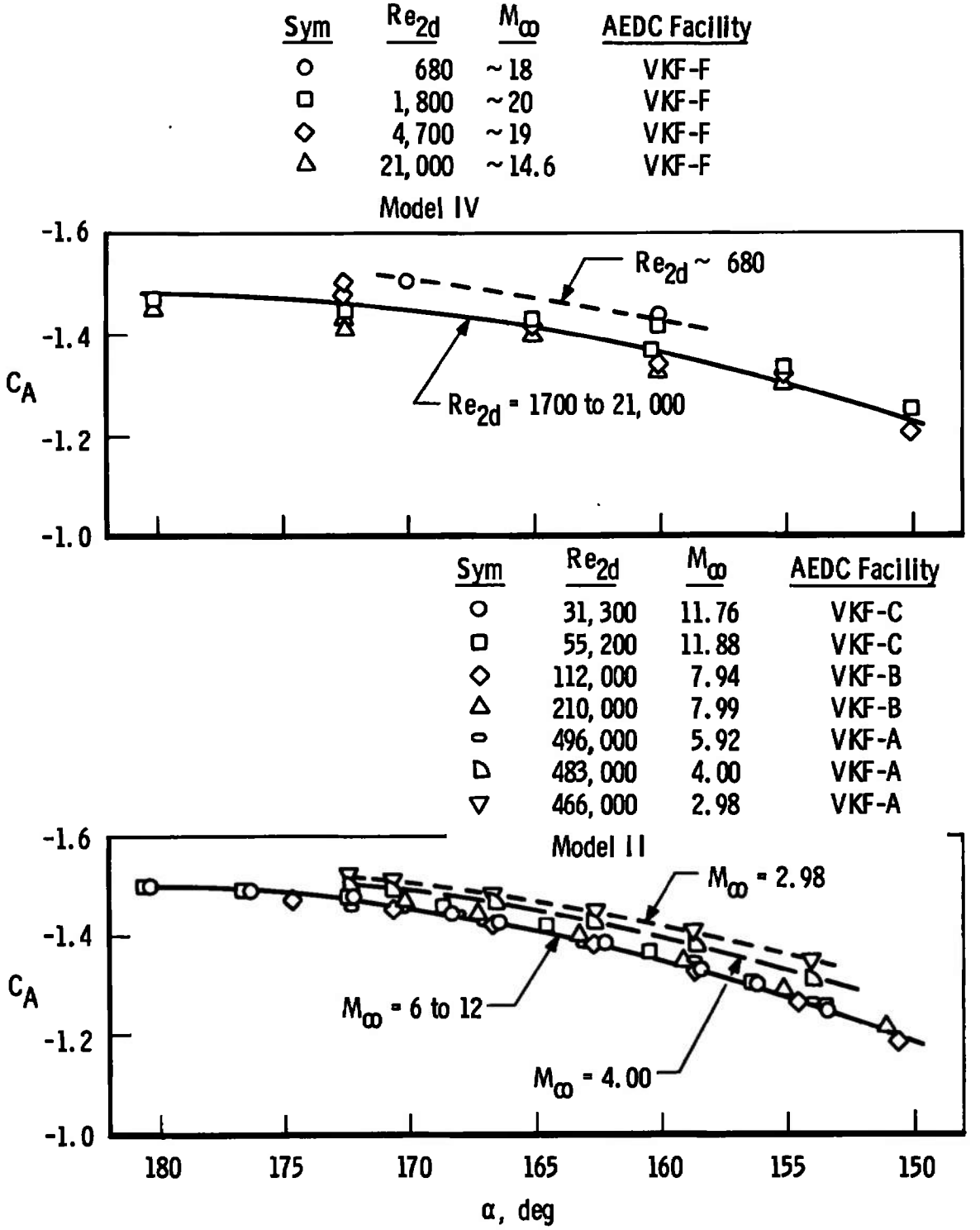

d. Variation of C_A with α, Asymmetrical Model

Fig. II-2 Continued

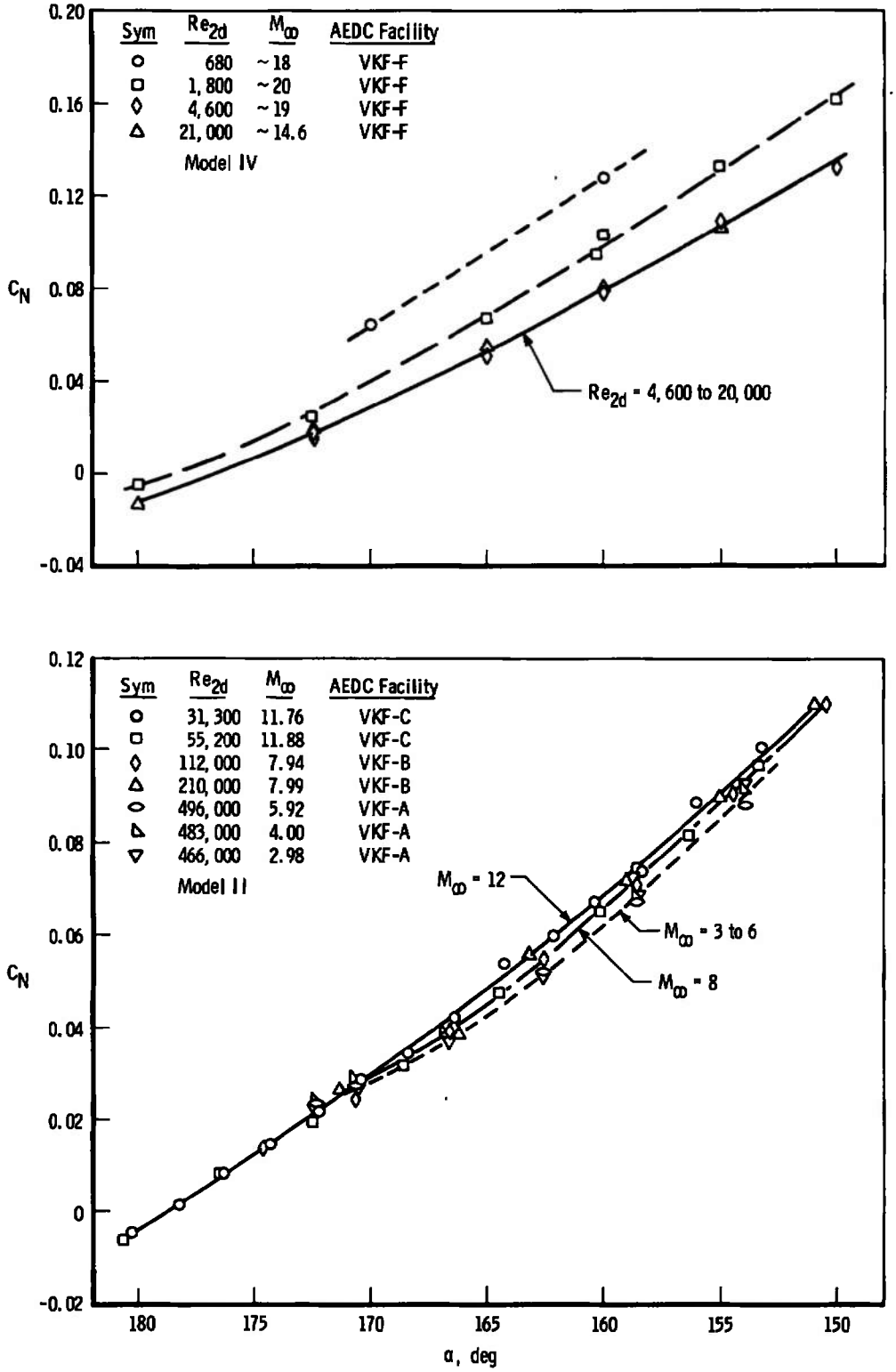

e. Variation of C_N with α, Asymmetrical Model

Fig. II-2 Continued

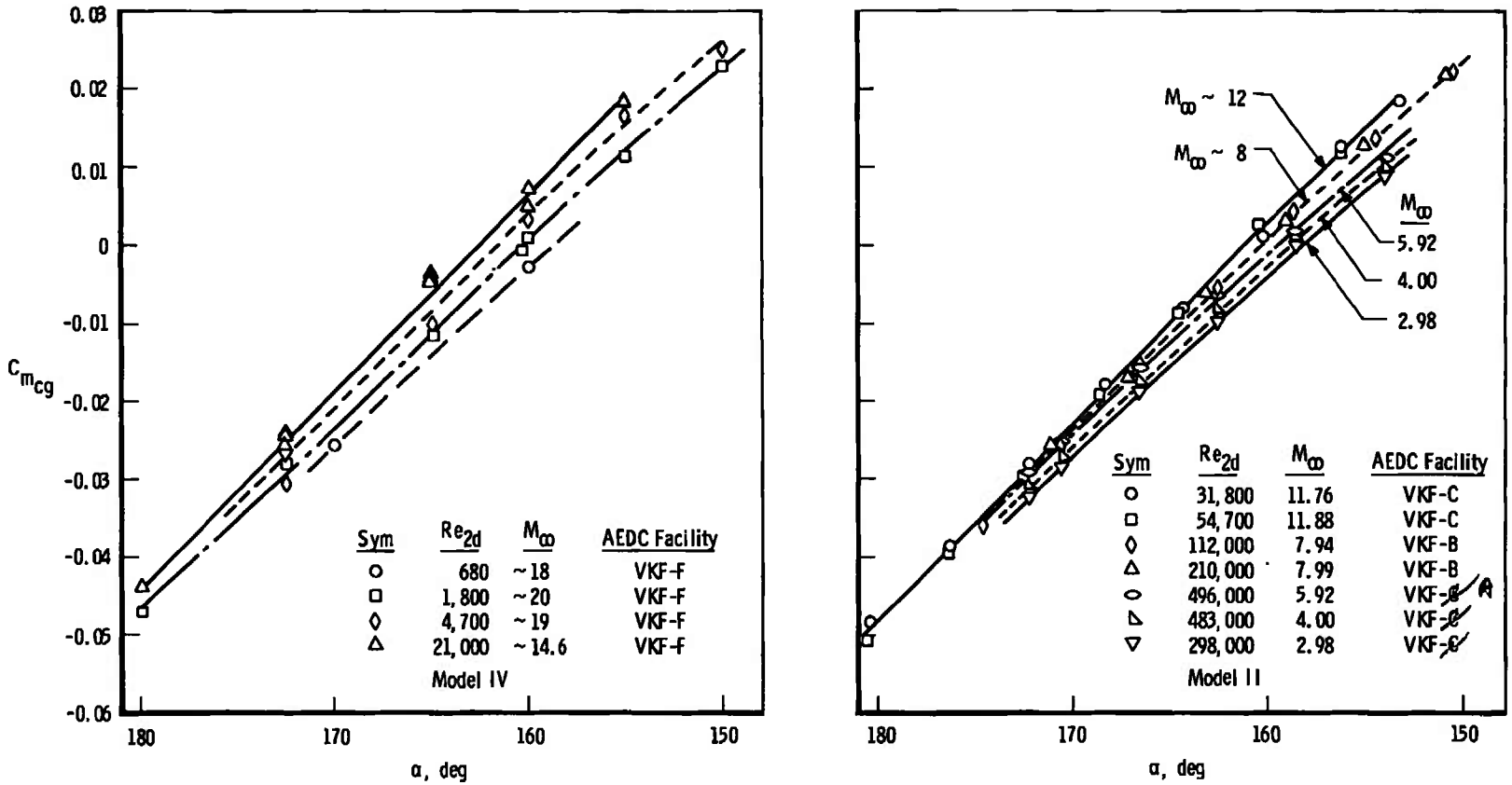

f. Variation of $C_{m_{cg}}$ with α, Asymmetrical Wavy Model

Fig. II-2 Concluded

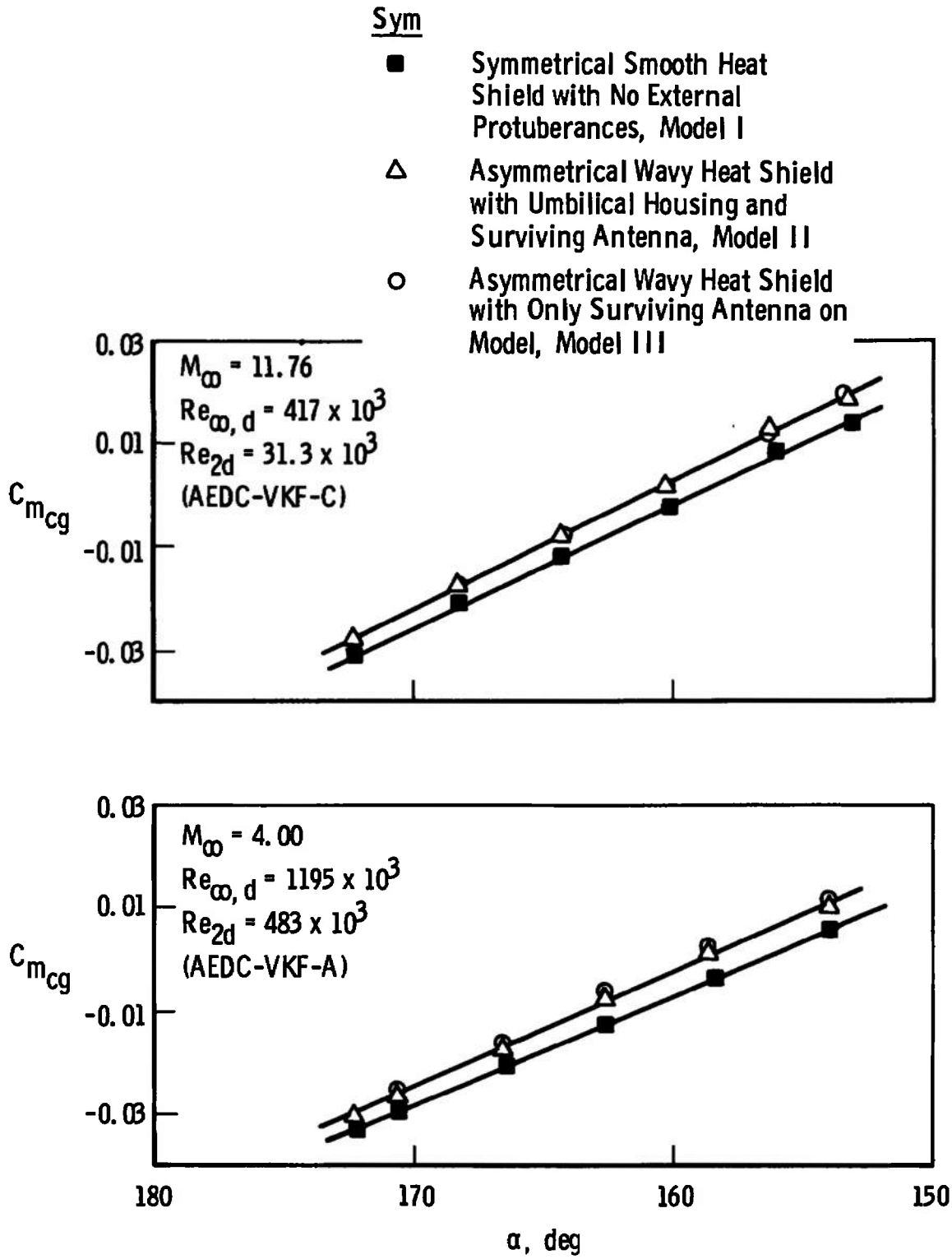

Fig. II-3 Effect of Protuberances

TABLE I
POSTFLIGHT (AS-202) WIND TUNNEL PROGRAM

(1) Effect of Asymmetry Heat Shield and Simulated Pressure Pads	AEDC-VKF Tunnels A, B, C, and F M_∞ = 3, 4, 8, 12, 14.6, 19 to 20
(2) Effect of Flight Angle	α = 180 to 150 deg (All Tunnels)
(3) Mach Number Effects	M_∞ = 3, 4, 6, 8, 10, 12, 14.6, 19 to 20
(4) Effect of Reynolds Number	Re_{2d} = 29 to 500,000 (All Tunnels)
(6) Possible Sting Effects	M_∞ ~ 8 AEDC-VKF Range G AEDC-VKF Tunnel B

TABLE II
NOMINAL TEST FLOW CONDITIONS

VKF Facility	p_o, psia	T_o, °K	M_∞	$Re_{\infty d}$	Re_{2d}
A	94	345	6.0	1900×10^3	500×10^3
	21	310	4.0	1200	480
	9	310	3.0	870	470
B	600	730	8.0	1800	210
	300	700	8.0	1000	110
	175	690	8.0	590	65
	100	670	8.0	360	38
C	2020	1270	12.0	730	55
	1120	1270	12.0	420	30
F	6000	2000	14.6	380	21.0
	6500	2350	19	110	4.7
	6500	3500	20	50	1.8
	3300	5000	18	14	0.68
L	25	1660	9.4	1.28	0.16
	25	1660	9.4	0.96	0.12
	18	3100	10.2	0.31	0.04
	18	3100	10.2	0.23×10^3	0.03×10^3
	Velocity		M_∞	$Re_{\infty d}$	Re_{2d}
G	6700		~6	240×10^3	80×10^3
	9700		~8.5	170	40
	6600		~6	120	40
	9300		~8	90	20
	9700		~8.5	50	10

TABLE III
TABULATED BASIC WIND TUNNEL DATA

Model Configuration

I. Summetrical Smooth Heat Shield with No External Protuberances

II. Asymmetrical Wavy Heat Shield with Umbilical Housing and Surviving Antenna

III. Asymmetrical Wavy Heat Shield with Only Surviving Antenna on Model

IV. Asymmetrical Wavy Heat Shield with Only Umbilical Housing on Model

Facility	Model	M_∞	$Re_{\infty,d} \times 10^{-3}$	$Re_{2d} \times 10^{-3}$	α, deg	$-C_A$	C_N	$C_{m_{cg}}$	L/D
VKF-A	I	2.98	868	466	154	1.306	0.0957	0.0038	0.3999
					158.5	1.368	0.0720	0.0053	0.3339
					162.6	1.409	0.0528	-0.0141	0.2732
					166.6	1.436	0.0395	-0.0224	0.2096
					170.6	1.463	0.0290	-0.0306	0.1456
					172.2	1.468	0.0247	-0.0339	0.1192
		4.00	1195	483	154	1.267	0.09420	0.0058	0.3989
					158.5	1.336	0.07137	-0.0038	0.3329
					162.6	1.382	0.05447	-0.0123	0.2715
					166.5	1.416	0.04187	-0.0207	0.2082
					170.6	1.442	0.03062	-0.0295	0.1445
					172.2	1.450	0.02538	-0.0330	0.1186

TABLE III (Continued)

Facility	Model	M_∞	$Re_{\infty,d} \times 10^{-3}$	$Re_{2d} \times 10^{-3}$	α, deg	$-C_A$	C_N	$C_{m_{cg}}$	L/D
VKF-A	II	2.98	868	466	154	1.345	0.09251	0.0088	0.4043
					158.6	1.406	0.06823	-0.0001	0.3370
					162.6	1.447	0.05088	-0.0097	0.2747
					166.6	1.478	0.03733	-0.0188	0.2114
					170.6	1.504	0.02742	-0.0285	0.1466
					172.3	1.514	0.02375	-0.0325	0.1195
	II	4.00	1195	483	154	1.311	0.09160	0.0102	0.4032
					158.6	1.379	0.06897	0.0010	0.3354
					162.6	1.427	0.05275	-0.0080	0.2733
					166.6	1.463	0.03945	-0.0174	0.2096
					170.6	1.490	0.02872	-0.0270	0.1457
					172.3	1.500	0.02338	-0.0310	0.1195
	II	5.92	1900	496	154	1.262	0.08804	0.0112	0.4034
					158.6	1.332	0.06773	0.0018	0.3351
					162.6	1.379	0.05265	-0.0065	0.2722
					166.6	1.419	0.03886	-0.0157	0.2093
					170.6	1.448	0.02769	-0.0253	0.1457
					172.3	1.456	0.02379	-0.0293	0.1195
	III	2.98	868	466	154	1.340	0.09259	0.0097	0.4042
					158.6	1.403	0.06909	0.0008	0.3366
					162.6	1.447	0.05192	-0.0086	0.2742
					166.6	1.480	0.03989	-0.0177	0.2096
					170.6	1.508	0.02791	-0.0268	0.1466

TABLE III (Continued)

Facility	Model	M_∞	$Re_{\infty,d} \times 10^{-3}$	$Re_{2d} \times 10^{-3}$	α, deg	$-C_A$	C_N	$C_{m_{cg}}$	L/D
VKF-A	III	4.00	1195	483	154	1.304	0.09240	0.0111	0.4025
					158.6	1.367	0.07082	0.0020	0.3340
					162.6	1.411	0.05310	-0.0068	0.2727
					166.6	1.452	0.04200	-0.0164	0.2079
					170.6	1.480	0.03076	-0.0254	0.1444
VKF-B	I	7.88	362	38.3	150.2	1.151	0.1183	0.0183	0.4445
					154.2	1.221	0.0979	0.0099	0.3888
					157.2	1.275	0.0851	0.0030	0.3440
					160.2	1.318	0.0715	-0.0037	0.3000
					164.2	1.357	0.0486	-0.0139	0.2443
					168.2	1.393	0.0338	-0.0229	0.1834
					174.2	1.430	0.0169	-0.0364	0.0895
	I	7.94	964	112	150.4	1.173	0.1144	0.0180	0.4455
					154.5	1.244	0.0936	0.0089	0.3881
					158.5	1.309	0.0757	-0.0008	0.3279
					162.6	1.364	0.0555	-0.0107	0.2695
					166.6	1.403	0.0427	-0.0202	0.2063
					170.6	1.431	0.0279	-0.0298	0.1458
					172.6	1.440	0.0202	-0.0345	0.1154
VKF-B	I	7.99	1810	210	150.9	1.180	0.1161	0.0171	0.4343
					155.0	1.252	0.0950	0.0078	0.3770
					159.1	1.316	0.0758	-0.0022	0.3176
					163.1	1.368	0.0573	-0.0118	0.2577
					167.2	1.406	0.0431	-0.0210	0.1959
					171.2	1.438	0.0293	-0.0308	0.1340

TABLE III (Continued)

Facility	Model	M_∞	$Re_{\infty, d} \times 10^{-3}$	$Re_{2d} \times 10^{-3}$	α, deg	$-C_A$	C_N	$C_{m_{cg}}$	L/D
VKF-B	II	7.88	362	38.3	150.1	1.174	0.1157	0.0229	0.4505
					154.2	1.251	0.0928	0.0145	0.3959
					157.2	1.302	0.0819	0.0081	0.3491
					160.2	1.344	0.0637	0.0007	0.3076
					164.2	1.397	0.0495	-0.0092	0.2448
					168.2	1.433	0.0341	-0.0189	0.1845
					172.2	1.451	0.0172	-0.0302	0.1252
	II	7.94	964	112	150.5	1.183	0.1099	0.0222	0.4500
					154.5	1.262	0.0904	0.0138	0.3916
					158.6	1.326	0.0713	0.0046	0.3320
					162.6	1.379	0.0552	-0.0054	0.2703
					166.6	1.421	0.0398	-0.0154	0.2119
					170.6	1.449	0.0247	-0.0259	0.1485
					174.6	1.468	0.0136	-0.0359	0.0855
	II	7.99	1810	210	151.0	1.209	0.1099	0.0217	0.4418
					155.1	1.284	0.0898	0.0127	0.3822
					159.1	1.347	0.0719	0.0032	0.3213
					163.2	1.397	0.0559	-0.0063	0.2588
					167.2	1.441	0.0388	-0.0172	0.1985
					171.2	1.470	0.0266	-0.0257	0.1355
	I	7.88	362	38.3	155.9	---	---	0.0033	---
					157.95	---	---	-0.0009	---
					159.4	---	---	-0.0042	---
					160.9	---	---	-0.0077	---
					162.9	---	---	-0.0124	---

TABLE III (Continued)

Facility	Model	M_∞	$Rc_{\infty, d} \times 10^{-3}$	$Re_{2d} \times 10^{-3}$	α, deg	$-C_A$	C_N	$C_{m_{cg}}$	L/D
VKF-B	I	7.91	590	64.6	157.35	---	---	0.0006	---
					158.8	---	---	-0.0021	---
					159.4	---	---	-0.0033	---
					160.0	---	---	-0.0045	---
					161.33	---	---	-0.0076	---
	I	7.95	1100	120	157.75	---	---	0	---
					158.92	---	---	-0.0022	---
					159.4	---	---	-0.0031	---
					160.15	---	---	-0.0043	---
					161.4	---	---	-0.0070	---
	I	7.99	1800	192	158.9	---	---	-0.0019	---
					159.4	---	---	-0.0033	---
					159.9	---	---	-0.0039	---
					160.65	---	---	-0.0053	---
					161.10	---	---	-0.0063	---
VKF-B	II	7.88	362	38.3	158.9	---	---	0.0025	---
					160.4	---	---	-0.0009	---
					161.4	---	---	-0.0031	---
					162.9	---	---	-0.0065	---
					163.9	---	---	-0.0089	---
	II	7.91	590	64.6	159.05	---	---	0.0035	---
					160.95	---	---	-0.0015	---
					161.68	---	---	-0.0031	---
					162.95	---	---	-0.0061	---
					163.8	---	---	-0.0081	---

TABLE III (Continued)

Facility	Model	M_∞	$Re_{\infty, d} \times 10^{-3}$	$Re_{2d} \times 10^{-3}$	α, deg	$-C_A$	C_N	$C_{m_{cg}}$	L/D
VKF-B	II	7.95	1100	120	159.2	---	---	0.0027	---
					161.1	---	---	-0.0014	---
					161.95	---	---	-0.0033	---
					162.05	---	---	-0.0037	---
					163.0	---	---	-0.0058	---
	II	7.99	1800	192	160.75	---	---	-0.0003	---
					161.75	---	---	-0.0026	---
					162.20	---	---	-0.0036	---
					163.10	---	---	-0.0056	---
					163.60	---	---	-0.0067	---
VKF-C	I	11.76	417	31.30	153.1	1.219	0.1040	0.0141	0.4049
					156.1	1.267	0.0904	0.0083	0.3601
					160.1	1.322	0.0702	-0.0024	0.3024
					164.3	1.380	0.0528	-0.0121	0.2410
					168.2	1.419	0.0378	-0.0211	0.1820
					172.2	1.441	0.0224	-0.0312	0.1210
					176.3	1.450	0.0133	-0.0402	0.0559
					180.3	1.450	-0.0007	-0.0480	-0.0051
	I	11.88	746	55.20	153.5	1.222	0.0988	0.0134	0.4022
					156.4	1.272	0.0857	0.0061	0.3584
					160.5	1.332	0.0671	-0.0034	0.2986
					164.6	1.380	0.0509	-0.0141	0.2371
					168.5	1.420	0.0341	-0.0228	0.1790
					172.4	1.446	0.0230	-0.0322	0.1169
					176.5	1.453	0.0130	-0.0408	0.0528
					180.6	1.456	-0.0014	-0.0497	-0.0100

TABLE III (Continued)

Facility	Model	M_∞	$Re_{\infty,d} \times 10^{-3}$	$Re_{2d} \times 10^{-3}$	α, deg	$-C_A$	C_N	$C_{m_{cg}}$	L/D
VKF-C	I	11.76	423	31.80	153.3	1.241	0.1000	0.0185	0.4064
					156.3	1.291	0.0846	0.0127	0.3631
					160.3	1.349	0.0670	0.0013	0.3023
					164.3	1.404	0.0456	-0.0082	0.2456
					168.3	1.442	0.0308	-0.0178	0.1851
					172.3	1.458	0.0138	-0.0281	0.1245
					176.3	1.480	0.0079	-0.0387	0.0585
					180.4	1.480	-0.0063	-0.0484	-0.0031
	II	11.88	739	54.70	153.4	1.253	0.0964	0.0185	0.4075
					156.4	1.302	0.0816	0.0118	0.3650
					160.4	1.366	0.0651	0.0025	0.3024
					164.5	1.414	0.0475	-0.0087	0.2416
					168.6	1.454	0.0319	-0.0192	0.1791
					172.5	1.480	0.0197	-0.0298	0.1176
					176.5	1.489	0.0083	-0.0394	0.0555
					180.6	1.495	-0.0061	-0.0507	-0.0067
	III	11.76	417	31.30	153.4	1.244	0.1002	0.0190	0.4047
					156.3	1.286	0.0849	0.0115	0.3623
					160.3	1.354	0.0676	0.0023	0.3023
					164.3	1.399	0.0514	-0.0073	0.2414
					168.4	1.444	0.0317	-0.0183	0.1818
VKF-F	I	18.02	11.66	0.670	180	1.584	---	-0.0530	---
		18.71	12.05	0.681	170	1.47	0.0605	-0.0285	0.1265
		18.50	14.55	0.714	160	1.385	0.1330	-0.0068	0.2589
		19.85	44.50	1.678	180	1.439	-0.0001	-0.0487	---
		19.62	45.60	1.756	172.5	1.447	0.0298	-0.0322	0.1108

TABLE III (Continued)

Facility	Model	M_∞	$Re_{\infty,d} \times 10^{-3}$	$Re_{2d} \times 10^{-3}$	α, deg	$-C_A$	C_N	$C_{m_{cg}}$	I./D
VKF-F	I	19.63	45.25	1.615	165	1.430	0.0633	-0.0163	0.2210
		20.30	59.20	2.060	160.3	1.375	0.0850	-0.0037	0.2898
		20.35	57.48	1.960	155	1.250	0.1258	0.0089	0.3493
		19.91	45.15	1.707	150	1.180	0.1522	0.0198	0.4126
		14.37	434.1	24.82	180	1.425	0	-0.0482	---
		14.56	381.2	21.55	165	1.300	0.0550	-0.0139	0.2232
		14.55	440.7	23.94	165	1.350	0.0566	-0.0143	0.2235
	IV	17.81	11.60	0.703	170	1.507	0.0640	-0.0257	0.1282
		18.28	12.90	0.690	160	1.437	0.1283	-0.0027	0.2600
		19.83	47.45	1.813	180	1.472	-0.0052	-0.0470	-0.0035
		20.33	58.70	1.978	172.5	1.455	0.0251	-0.0283	0.1141
		19.96	47.50	1.734	165	1.430	0.0669	-0.0117	0.2189
		19.87	47.75	1.757	160	1.414	0.1030	0.0009	---
		19.34	33.90	1.464	160.3	1.363	0.0950	-0.0008	0.2813
		19.88	47.45	1.851	155	1.335	0.133	0.0115	0.3504
		20.01	45.40	1.748	150	1.252	0.162	0.0230	0.4169
		17.84	68.22	3.050	165	1.420	0.0504	-0.0093	0.2303
		20.42	71.75	2.533	160	1.409	0.0874	0.0023	0.2954
		18.60	128.4	4.917	172.5	1.473	0.0150	-0.0267	0.1213
		18.74	133.2	4.874	172.5	1.498	0.0166	-0.0307	0.1203
		18.62	139.0	5.099	165	1.427	0.0511	-0.0100	0.2299
		19.12	157.6	5.224	160	1.340	0.0777	0.0032	0.2997
		18.68	135.4	5.120	155	1.317	0.1087	0.0169	0.3695
		18.68	135.4	5.077	150	1.205	0.1324	0.0249	0.4396
		14.59	401.8	22.58	180	1.450	-0.0126	-0.0439	---
		14.80	381.4	20.33	172.5	1.435	0.0152	-0.0243	0.1210

TABLE III (Continued)

Facility	Model	M_∞	$Re_{\infty,d} \times 10^{-3}$	$Re_{2d} \times 10^{-3}$	α, deg	$-C_A$	C_N	$C_{m_{cg}}$	L/D
VKF-F	IV	14.76	486.0	24.59	172.5	1.460	0.0163	-0.0262	0.1196
		14.67	408.7	22.44	172.5	1.415	0.0180	-0.0240	0.1187
		14.58	319.8	18.07	165	1.419	0.0553	-0.0042	0.2266
		14.92	373.7	19.40	165	1.385	0.0531	-0.0049	0.2273
		14.73	358.0	19.84	165	1.398	0.0545	-0.0040	0.2266
		14.92	363.0	19.42	160	1.340	0.0806	0.0072	0.2974
		14.77	299.5	16.60	160	1.330	0.0793	0.0046	0.2979
		14.70	374.2	20.36	155	1.303	0.1067	0.0185	0.3701
VKF-L	I	10.15	0.233	0.0289	155	1.590	0.357	0.0007	0.2189
					160	1.670	0.287	-0.0127	0.1808
					165	1.750	0.216	-0.0225	0.1399
					170	1.800	0.145	-0.0300	0.0944
					175	1.820	0.072	-0.0440	0.0478
					180	1.825	0	-0.0617	0
		10.15	0.310	0.0385	155	1.520	0.310	+0.0059	0.2396
					160	1.600	0.255	-0.0105	0.1934
					165	1.670	0.195	-0.0198	0.1466
					170	1.710	0.130	-0.0260	0.0830
					175	1.740	0.070	-0.0400	0.0471
					180	1.750	0	-0.0592	0
		9.37	0.960	0.118	155	1.400	0.225	-0.0119	0.2843
					160	1.470	0.177	-0.0016	0.2333
					165	1.530	0.135	-0.0131	0.1756

TABLE III (Continued)

Facility	Model	M_∞	$Re_{\infty,d} \times 10^{-3}$	$Rc_{2d} \times 10^{-3}$	α, deg	$-C_A$	C_N	$C_{m_{cg}}$	L/D
VKF-L	I	9.37	0.960	0.118	170	1.580	0.090	-0.0260	0.1182
					175	1.610	0.045	-0.0400	0.0594
					180	1.630	0	-0.0552	0
		9.37	1.280	0.157	155	1.380	0.210	0.0122	0.2933
					160	1.450	0.177	-0.0010	0.2316
					165	1.510	0.138	-0.0117	0.1723
					170	1.570	0.095	-0.0260	0.1146
					175	1.600	0.048	-0.0400	0.0573
					180	1.610	0	-0.0545	0

TABLE III (Concluded)

Facility	Model	M_∞	$Rc_{\infty,d} \times 10^{-3}$	$Re_{2d} \times 10^{-3}$	α_E, deg	C_D	e/d	α_T, deg	Shot Number
VKF-G	I	8.57	55.0	13.0	169.8	1.446	0.0157	168.52	615
		8.46	52.0	12.3	166.6	1.418	0.0162	168.88	617
		8.16	89.6	21.1	---	---	0.0163	168.69	619
		8.66	160.0	35.9	166.5	1.416	0.0164	170.34	632
		8.37	52.4	12.5	---	---	0.0344	157.25	616
		8.72	53.7	12.4	168.2	1.430	0.0351	157.04	618
		8.38	90.9	21.2	---	---	0.0339	158.98	620
		8.19	86.2	20.3	---	---	0.0332	159.01	633
		8.52	51.9	12.3	174.0	1.460	0.0002	~180	614
		8.47	172	39.4	177.4	1.494	0.0001	~180	631
		5.93	80	23.8	165.7	1.372	0.0002	~180	600
		5.47	108	33.5	162.6	1.328	0.0005	~180	601
		5.88	241	71.5	172.9	1.437	0.0004	~180	602

TABLE IV
TYPICAL APOLLO MISSION AS-202 FLIGHT DATA

Altitude,‡ ft	Time,* sec	Velocity,+ fps	L/D	C_N/C_A	α_T, deg
397, 293	4350	27, 201	-0.4996	0.05790	155.4
363, 850	4370	27, 239	-1.2778	0.98088	155.2
348, 195	4380	27, 256	-0.0347	0.48258	155.5
342, 133	4384	27, 263	0.6247	-0.55835	154.9
333, 255	4390	27, 273	0.3528	-0.21549	154.6
327, 430	4394	27, 279	0.3989	-0.49305	154.9
321, 820	4398	27, 284	0.2689	-0.23335	156.1
319, 032	4400	27, 287	0.2748	-0.15894	156.6
316, 274	4402	27, 290	0.2982	-0.13276	157.7
313, 544	4404	27, 292	0.2904	-0.11296	158.9
310, 842	4406	27, 294	0.3017	-0.06333	159.7
308, 168	4408	27, 296	0.2483	-0.12424	160.4
305, 523	4410	27, 297	0.2601	-0.08263	161.5
303, 319	4414	27, 300	0.2536	-0.07934	161.4
292, 722	4420	27, 301	0.2838	-0.07688	160.2
285, 374	4426	27, 300	0.2852	-0.05323	161.2
280, 611	4430	27, 298	0.2631	-0.05585	162.1
275, 956	4434	27, 291	0.2858	-0.06901	160.5
269, 167	4440	27, 280	0.2646	-0.06061	161.8
258, 346	4450	27, 238	0.2819	-0.04831	161.5
238, 772	4470	26, 998	0.2628	-0.03897	163.6
224, 078	4490	26, 408	0.2693	-0.04538	162.6
215, 682	4510	25, 513	0.2703	-0.04622	162.9
213, 613	4530	24, 498	0.2723	-0.05420	162.0
216, 712	4550	23, 569	0.2746	-0.05682	162.0
223, 210	4570	22, 845	0.2747	-0.05725	162.1
231, 202	4590	22, 345	0.2787	-0.05460	162.2
239, 246	4610	22, 002	0.2785	-0.06094	161.6

‡Above ground

*Time zero is liftoff

+Relative to ground

TABLE IV (Continued)

Altitude,‡ ft	Time,* sec	Velocity,+ fps	L/D	C_N/C_A	α_T, deg
246, 379	4630	21, 779	0. 2846	-0. 06290	161. 0
247, 627	4634	21, 744	0. 2819	-0. 04349	162. 0
250, 948	4646	21, 650	0. 2849	-0. 05527	161. 2
251, 986	4650	21, 622	0. 2826	-0. 05615	161. 4
254, 632	4664	21, 531	0. 2831	-0. 03280	162. 5
254, 935	4666	21, 519	0. 3067	-0. 05132	160. 0
255, 473	4670	21, 496	0. 2613	-0. 01663	164. 4
256, 720	4688	21, 400	0. 2506	-0. 04062	164. 3
256, 740	4690	21, 389	0. 2613	-0. 03642	163. 6
256, 196	4704	21, 318	0. 2861	-0. 04946	161. 3
255, 592	4710	21, 287	0. 3075	-0. 04403	160. 4
253, 706	4722	21, 223	0. 2801	-0. 03156	162. 6
251, 940	4730	21, 178	0. 2848	-0. 03582	162. 1
247, 891	4744	21, 088	0. 2937	-0. 05203	160. 7
245, 810	4750	21, 044	0. 2917	-0. 05685	160. 6
241, 906	4760	20, 960	0. 2709	-0. 05377	162. 7
237, 494	4770	20, 854	0. 2910	-0. 05187	160. 8
231, 663	4782	20, 891	0. 2799	-0. 04491	162. 2
227, 368	4790	20, 557	0. 2878	-0. 05987	160. 6
217, 206	4808	20, 141	0. 2810	-0. 03703	162. 5
216, 041	4810	20, 084	0. 2831	-0. 05214	161. 4
214, 875	4812	20, 024	0. 2815	-0. 04269	162. 7
204, 428	4830	19, 359	0. 2826	-0. 05333	161. 4
198, 865	4840	18, 881	0. 2837	-0. 03686	162. 3
193, 639	4850	18, 338	0. 2830	-0. 04822	161. 5
186, 403	4866	17, 291	0. 2855	-0. 04214	161. 9
184, 859	4870	17, 004	0. 2850	-0. 04228	161. 7

TABLE IV (Concluded)

Altitude,‡ ft	Time,* sec	Velocity,+ fps	L/D	C_N/C_A	α_T, deg
178,648	4890	15,526	0.2865	-0.04568	161.6
176,254	4900	14,788	0.2862	-0.04943	161.3
174,135	4910	14,074	0.2866	-0.05372	161.8
172,509	4918	13,520	0.2872	-0.05908	162.0
170,018	4930	12,704	0.2919	-0.05001	161.3
167,838	4940	12,019	0.2959	-0.04478	161.5
165,487	4950	11,354	0.2984	-0.04733	161.0
161,723	4964	10,458	0.3026	-0.05163	161.1
159,874	4970	10,091	0.3037	-0.04248	160.8
156,439	4980	9,470	0.3060	-0.04606	161.0
152,569	4990	8,849	0.3033	-0.04362	160.9
145,313	5006	7,847	0.3080	-0.04318	161.2
143,342	5010	7,588	0.3083	-0.05173	159.9
134,044	5028	6,379	0.3117	-0.03978	160.5
132,984	5030	6,240	0.3117	-0.04886	160.0
122,279	5050	4,864	0.3152	-0.04973	160.5
116,879	5060	4,207	0.3105	-0.05273	160.1
111,386	5070	3,599	0.3311	-0.04139	159.9
104,652	5082	2,934	0.3194	-0.04974	159.6
100,062	5090	2,532	0.3344	-0.04599	159.0
98,902	5092	2,439	0.3388	-0.04260	159.6
88,321	5110	1,707	0.3528	-0.05008	158.2
76,090	5130	1,177	0.3429	-0.02321	160.6
63,666	5150	845	0.2210	-0.04026	168.2
51,048	5170	693	0.2522	-0.04282	163.6
39,559	5190	573	0.0000	0.00000	---
29,682	5210	484	0.2720	-0.02584	163.3
21,712	5230	320	0.1466	-0.24114	159.1

Security Classification

DOCUMENT CONTROL DATA - R & D

(Security classification of title, body of abstract and indexing annotation must be entered when the overall report is classified)

1. ORIGINATING ACTIVITY (Corporate author) Arnold Engineering Development Center ARO, Inc., Operating Contractor Arnold Air Force Station, Tennessee	2a. REPORT SECURITY CLASSIFICATION UNCLASSIFIED 2b. GROUP N/A

3 REPORT TITLE

POSTFLIGHT (AS-202) APOLLO COMMAND MODULE AERODYNAMIC SIMULATION TESTS

4. DESCRIPTIVE NOTES (Type of report and inclusive dates)

December 1966 to May 1967 - Final Report

5. AUTHOR(S) (First name, middle initial, last name)

B. J. Griffith and D. E. Boylan, ARO, Inc.

6 REPORT DATE March 1968	7a. TOTAL NO. OF PAGES 81	7b. NO. OF REFS 13
8a. CONTRACT OR GRANT NO. AF 40(600)-1200 b. PROJECT NO. c. System 920E d.	9a. ORIGINATOR'S REPORT NUMBER(S) AEDC-TR-67-238 9b. OTHER REPORT NO(S) (Any other numbers that may be assigned this report) N/A	

10 DISTRIBUTION STATEMENT

This document has been approved for public release and sale; its distribution is unlimited.

11 SUPPLEMENTARY NOTES Available in DDC	12. SPONSORING MILITARY ACTIVITY Arnold Engineering Development Center, Air Force Systems Command Arnold Air Force Station, Tennessee

13 ABSTRACT A comprehensive postflight wind tunnel investigation of the Apollo Command Module was conducted to resolve several anomalies between flight (AS-202) and preflight aerodynamic data. Attention was focused on (1) simulating the actual vehicle "as flown", (2) obtaining consistent pitch plane force measurements in the angle-of-attack range $150 \leq \alpha \leq 180$ deg, (3) the effect of Mach number over a range of 3 to 20, (4) the effect of Reynolds number, and (5) possible sting effects. Results indicated that prior failure to duplicate the asymmetrical wavy heat shield in preflight testing resulted in a significant error in trim angle-of-attack prediction. In addition, a strong viscous influence was found to extend down to an altitude of about 220,000 ft. Also, a Mach number influence to a value of about 14 was found which is substantially higher than previous blunt body investigations have indicated.

DD FORM 1 NOV 65 1473

Security Classification

14 KEY WORDS	LINK A		LINK B		LINK C	
	ROLE	WT	ROLE	WT	ROLE	WT
postflight testing						
Apollo Command Module						
spacecrafts						
sting effects						